



HAL
open science

Pyrene/coumarine-subphthalocyanine conjugates as light harvesting systems with intramolecular energy transfer

Vivian Lioret, Yoann Rousselin, Richard Decreau

► To cite this version:

Vivian Lioret, Yoann Rousselin, Richard Decreau. Pyrene/coumarine-subphthalocyanine conjugates as light harvesting systems with intramolecular energy transfer. *Dyes and Pigments*, 2020, 183, pp.108696. 10.1016/j.dyepig.2020.108696 . hal-03476777

HAL Id: hal-03476777

<https://hal.science/hal-03476777>

Submitted on 13 Dec 2021

HAL is a multi-disciplinary open access archive for the deposit and dissemination of scientific research documents, whether they are published or not. The documents may come from teaching and research institutions in France or abroad, or from public or private research centers.

L'archive ouverte pluridisciplinaire **HAL**, est destinée au dépôt et à la diffusion de documents scientifiques de niveau recherche, publiés ou non, émanant des établissements d'enseignement et de recherche français ou étrangers, des laboratoires publics ou privés.

Manuscript Details

Manuscript number	DYPI_2020_1212
Title	Pyrene/coumarine-subphthalocyanine conjugates as light harvesting systems with intramolecular energy transfer
Article type	Research paper

Abstract

A series of subphthalocyanine-antenna dyads have been successfully designed, synthesized and characterized by ¹H-NMR, ¹³C-NMR, high-resolution mass spectroscopy, and X-ray diffraction studies with one dyad. Pyrene and coumarine have been appended at the axial position of the subphthalocyanine scaffold using different types of linkers. Photophysical properties of the new compounds have been measured in toluene, tetrahydrofuran, chloroform, dimethyl sulfoxide and methanol. Energy transfer efficiencies between antenna and the subphthalocyanine platform have been investigated and almost quantitative energy transfer occurs in the antenna-platform 5.

Keywords	subphthalocyanine; pyrene; coumarine; dyad; fluorescence; intramolecular energy transfer
Corresponding Author	Richard decaeu
Corresponding Author's Institution	University of Burgundy Franche Comté
Order of Authors	Vivian Lioret, Yoann Rousselin, Richard decaeu
Suggested reviewers	Mogens Nielsen, Timothy Bender, Christopher Ziegler

Submission Files Included in this PDF

File Name [File Type]

- 5-Cover Letter.pdf [Cover Letter]
- 5-Highlight.pdf [Highlights]
- 05.draft.pdf [Manuscript File]
- 5-checkcif(1).pdf [Figure]
- 5-declaration-of-competing-interests(1).pdf [Conflict of Interest]
- 5-SI_final version.pdf [Supplementary Material]

Submission Files Not Included in this PDF

File Name [File Type]

- 5-Graphical Abstract.PNG [Graphical Abstract]

To view all the submission files, including those not included in the PDF, click on the manuscript title on your EVISE Homepage, then click 'Download zip file'.

Dyes and Pigments
Editors of Dyes and Pigments

Dijon, May 27th, 2020

Dear Editor,

We would like to submit a manuscript entitled "Pyrene/coumarine-subphthalocyanine conjugates as light harvesting systems with intramolecular energy transfer" for publication in *Dyes and Pigments*.

This study reports the syntheses of several dyads of fluorophores and subsequent studies of intramolecular energy transfers. In such dyads the acceptor is a subphthalocyanine, the donor is either a coumarin or a pyrene, and the nature of the linker between both has been varied. Next, upon careful purification and characterization of the conjugates including X-ray diffraction studies for two candidates, subsequent photophysical studies have been engaged. Upon fluorescence spectroscopy, fluorescence quantum yields have been measured and subsequent energy transfer between both moieties within each dyad has been also measured. Up to five different organic solvents have been examined to carry out such studies. One out of three dyads underwent almost quantitative energy transfer efficiency (E.T.E.).

Overall this study is a blend of organic synthesis of new subphthalocyanine-based fluorophore dyads, and photophysical studies addressing the energy transfer between two fluorophores.

We hope this study will be of interest for readers of *Dyes and Pigments*.

Sincerely,

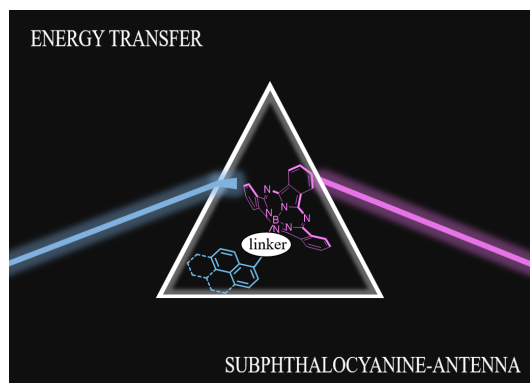
Richard A. Decréau

Dr Richard A. Decréau ; Associate Professor ; Institut de Chimie Moléculaire de l'Université de Bourgogne (ICMUB), UMR 6302 CNRS-Université de Bourgogne, BP 47 870, F-21 078 Dijon Cedex, France ; Richard.Decreau@u-bourgogne.fr

1
2
3 **Highlight**
4

5
6
7 Required : 85 characters. Here : 85 characters
8

9 The Energy Transfer Efficiency was studied in four new subphthalocyanine-fluorophore
10 conjugates
11



Pyrene/coumarine-subphthalocyanine conjugates as light harvesting systems with intramolecular energy transfer

Vivian Lioret^a, Yoann Rousselin^a, Richard A. Decréau^{a,*}

^a ICMUB Institute, University Bourgogne – Franche Comté, 9 Avenue Alain Savary, Sciences Mirande, 21078 Dijon, France

* Corresponding author. E-mail address: Richard.Decreau@u-bourgogne.fr (R.A. Decréau).

ABSTRACT

A series of subphthalocyanine-antenna dyads have been successfully designed, synthesized and characterized by ¹H-NMR, ¹³C-NMR, high-resolution mass spectroscopy and X-ray diffraction for some of them. Pyrene and coumarine have been appended at the axial position of the subphthalocyanine scaffold using different types of linkers. Photophysical properties of the new compounds have been measured in toluene, tetrahydrofuran, chloroform, dimethyl sulfoxide and methanol. Energy transfer efficiencies between antenna and the subphthalocyanine platform have been investigated and almost quantitative energy transfer occurs in the antenna-platform **5**.

Keywords: Subphthalocyanine, Pyrene, Coumarine, Dyad, Fluorescence, Intramolecular Energy Transfer

1. Introduction

Energy transfer is a crucial process in nature, but also in more artificial applications, such as the conversion of solar energy into electricity, in optoelectronic devices[1] or in the detection of analytes[2, 3]. Over the past decades, this area of research has become a fertile field for the association of two or more chromophores together. The interaction of different partners and the exchange of energy between them has become an attractive investigation domain. Numerous conjugated polyazamacrocycles, such as porphyrins[4, 5], phthalocyanines[6] or naphthalocyanines[4] have been employed as partners for photophysical or electronic studies. Among them, subphthalocyanines, which are lower homologues of phthalocyanines having a central Boron (III) atom, are another important class of chromophores. They are conic-shaped macrocycles, with a 14- π electron aromatic core. This scaffold is used in many fields, such as organic material[7], photodynamic therapy[8] or optoelectronic[9, 10]. Most functionalizations of the SubPc moieties are done by substitution of the axial halogen.

In order to study energy transfers with subphthalocyanines, pyrene and coumarine have been chosen to absorb light in the UV-blue region of the visible spectrum. Although a few pyrene-SubPc dyads have already been described in the literature[11], we specifically investigated the efficiency of the energy transfer between these two units as a function of the nature of the linker. For this purpose, the SubPc platform has been functionalized at the axial position [12, 13] (and not at the iso-indolic position, which may otherwise affect the electronic properties of the

platform) by the pyrene, choosing chemical modifications, such as a triple bond, a B-O-R or a B-O-CH₂-R as a linker. Coumarine was also linked to the SubPc platform by a B-O-R link. The photophysical behavior of these antenna-SubPc dyads were explored using fluorescence spectroscopy. SubPc are also known to be good singlet oxygen generator under light exposure[14], yet, we did not measured their ability to perform such generation.

2. Experimental

2.1. Materials and equipments

¹H and ¹³C NMR spectra were recorded on a Bruker Avance III 500 MHz spectrometer. Chemical shifts are expressed in parts per million (ppm) from the residual non-deuterated solvent signal. J values are expressed in Hz. HPLC-MS analyses were performed on a Thermo-Dionex Ultimate 3000 instrument equipped with a diode array detector (Thermo-Dionex, FLD 3400-RS). High-resolution mass spectra (HRMS) were recorded on a LTQ Orbitrap XL (THERMO) equipped with an electrospray (ESI) source. For single crystal X-ray diffraction analyzes, all experimental data procedure and refinement are detailed in Supplementary Information. Data CCDC- 2005981 and 2005982 contain the supplementary crystallographic data for this paper for compound **4** and **6** respectively. These data can be obtained free of charge from The Cambridge Crystallographic Data Centre via www.ccdc.cam.ac.uk/data_request/cif

2.2. Fluorescence quantum yield

UV-Visible measurements were performed on an Agilent Cary 60 using a glass cuvette (1x1x3 cm). Fluorescence spectroscopic studies (emission/excitation spectra) were performed on a HORIBA Jobin Yvon Fluorolog spectrophotometer (software FLuorEssence) at 25°C (using a temperature control system combined with water circulation), with standard fluorometer cells (Labbox, LB Q, light path: 10 mm, width: 10 mm, chamber volume: 3.5 mL). Fluorescence quantum yields were calculated by relative method using rhodamine 6G in ethanol ($\Phi_F = 0.96$, 488 nm). Emission Spectra were recorded for an absorbance at excitation wavelength comprised between 0.02 and 0.09. Fluorescence quantum yield (Φ_F) were determined using the following equation:

$$\Phi_F = \Phi_F(Std) \times \left(\frac{\eta}{\eta(Std)} \right)^2 \times \left(\frac{1 - 10^{-Abs}}{1 - 10^{-Abs(Std)}} \right) \times \left(\frac{A(Std)}{A} \right)$$

With:

Std corresponds to standard

Φ_F and $\Phi_F(Std)$: fluorescence quantum yields

η and $\eta(Std)$: refractive index of solvent

119
120
121 Abs and Abs (Std): absorbance at excitation wavelength (488 nm)

122 A and A (Std): areas under the fluorescence curves

123 2.3. Synthesis

124 2.3.1. Synthesis of compound **1**

125
126 To a solution of phthalonitrile (1.06 g, 8.27 mmol) in dry dichlorobenzene (DCB, 45
127 mL), under nitrogen atmosphere, was slowly added BCl₃ (20 mL, 1M in hexane, 20 mmol) and
128 the reaction was heated at 70°C to remove hexane. After 30 min at 70°C, a condenser was added
129 and the reaction mixture was heated at 180°C for 1.5 hours. The color went from light milky
130 yellow to dark purple. Then the reaction mixture was cooled down and a precipitate was formed.
131 The solid was filtrated, washed with methanol and pentane and dried under vacuum to afford
132 compound **1** (700 mg, 58%). ¹H NMR (500 MHz, CDCl₃, 300 K): δ (ppm) 7.95 (m, 6H), 8.90
133 (m, 6H). HR-MS ESI: m/z 431.0966 [M+H]⁺ (calcd for C₂₄H₁₃BCIN₆⁺: 431.0978). HP-LC
134 analysis: retention time 5.83.
135
136
137
138
139
140
141

142 2.3.2. Synthesis of compound **2**

143 1-pyrenecarboxaldehyde (1 g, 4.3 mmol) and dry THF (20 mL) were mixed together.
144 Sodium borohydride (165 mg, 4.3 mmol) was added in small portions, together with small
145 portions of methanol to help the solubilization (total volume of added methanol 10 mL). An
146 orange solution was obtained. The reaction was then quenched with a 2% concentrated
147 hydrochloric acid solution. The solvent was removed under reduced pressure. The white
148 powder obtained was dissolved in dichloromethane, washed with water and the organic phase
149 was dried with magnesium sulfate. The solvent was removed under reduced pressure and the
150 resulting solid was subjected to silica gel column chromatography (eluent: DCM) to afford
151 compound **2** (0.88 g, 88%). ¹H NMR (500 MHz, CDCl₃, 300 K): δ (ppm) 1.90 (s, 1H), 5.40 (s,
152 2H), 7.98 – 8.10 (m, 4H), 8.15 (m, 2H), 8.20 (m, 2H), 8.37 (d, *J* = 9.2 Hz, 1H). ¹³C NMR (125
153 MHz, CDCl₃, 300 K): δ (ppm) 64.04, 123.16, 124.88, 124.92, 125.13, 125.43, 125.46, 126.16,
154 126.20, 127.55, 127.64, 128.08, 128.97, 130.94, 131.41, 131.44, 133.92. HR-MS ESI: m/z
155 247.0762 [M+O-H]⁻ (calcd for C₁₇H₁₀O₂⁻: 247.0765). HP-LC analysis: retention time 4.78.
156
157
158
159
160
161

162 2.3.3. Synthesis of compounds **3**, **4** and **6**

163
164 *General procedure.* The synthetic method reported here to append aryloxy/alkoxy structures at
165 the axial position of the SubPc platform was reminiscent of that we reported for phenoxy
166 moieties.[15] To a solution of compound **1** (50 mg, 0,116 mmol) in toluene (5 mL) was added
167 the corresponding antenna (0,58 mmol). The reaction mixture was heated under refluxing
168 conditions during 2-5 days and monitored by LCMS. The solvent was then removed under
169 reduced pressure and the crude product was subjected to silica gel column chromatography.
170
171
172
173
174
175
176
177

178
179
180
181
182
183 **Compound 3**
184

185
186 Compound **3** was synthesized following the general procedure, where the chosen antenna was
187 compound **2** (134 mg). The reaction mixture was heated under refluxing conditions for 5 days.
188 Target compound **3** was obtained after purification of the crude product by silica gel column
189 chromatography using the DCM/MeOH mixture (95/5 vol.) as an eluent to afford the desired
190 product **3** (52 mg, 74%). ¹H NMR (500 MHz, CDCl₃, 300 K): δ (ppm) 3.40 (m, 2H), 5.29 (s,
191 1H), 7.08 (d, *J* = 7.8 Hz, 1H), 7.28 (d, *J* = 9.2 Hz, 1H), 7.75 – 7.88 (m, 10H), 7.99 (d, *J* = 7.6
192 Hz, 2H), 8.76 (m, 6H). ¹³C NMR (125 MHz, CDCl₃, 300 K): δ (ppm) 60.55, 122.09, 122.78,
193 124.28, 124.48, 124.86, 124.93, 125.24, 125.64, 126.89, 127.22, 127.35, 127.87, 129.69,
194 130.56, 130.64, 131.01, 131.15, 132.35, 151.43. HR-MS ESI: *m/z* 627.2069 [M+H]⁺ (calcd for
195 C₄₁H₂₄BN₆O⁺: 627.2099). HP-LC analysis: retention time 6.68 min.
196
197
198
199
200

201 **Compound 4**
202

203
204 Compound **4** was synthesized following the general procedure where the chosen antenna was
205 1-hydroxypyrene (127 mg). The reaction mixture was heated under refluxing conditions for 2
206 days. The final product was obtained after purification of the crude mixture by silica gel column
207 chromatography using DCM as an eluent to afford the desired product **4** (32 mg, 45%). ¹H
208 NMR (500 MHz, CDCl₃, 300 K): δ (ppm) 5.88 (d, *J* = 8.3 Hz, 1H), 6.88 (d, *J* = 9.1 Hz, 1H),
209 7.60 (dd, *J* = 8.7, 1.8 Hz, 2H), 7.74 (d, *J* = 1.7 Hz, 2H), 7.79 (t, *J* = 7.6 Hz, 1H), 7.86 – 7.91 (m,
210 7H), 7.93 (dd, *J* = 7.5, 1.2 Hz, 1H), 8.81 – 8.86 (m, 6H). ¹³C NMR (125 MHz, CDCl₃, 300 K):
211 δ (ppm) 116.13, 120.67, 122.41, 124.08, 124.20, 124.67, 125.21, 125.23, 125.44, 125.82,
212 126.11, 126.21, 127.19, 130.02, 131.13, 131.15, 131.36, 131.38, 147.10, 151.57. HR-MS ESI:
213 *m/z* 613.1908 [M+H]⁺ (calcd for C₄₀H₂₁BN₆O⁺: 613.1943). HP-LC analysis: retention time 7.36
214 min.
215
216
217
218
219

220 **Compound 6**
221

222
223 Compound **6** was synthesized following the general procedure, where the chosen antenna was
224 7-hydroxycoumarin (94 mg). The reaction mixture was heated under refluxing conditions for
225 2 days. Target compound **6** was obtained after subjecting the crude mixture to silica gel column
226 chromatography using DCM as an eluent to afford the desired product **6** (41 mg, 64%). ¹H
227 NMR (500 MHz, CDCl₃, 300 K): δ (ppm) 5.27 (d, *J* = 2.2 Hz, 1H), 5.33 (dd, *J* = 8.5, 2.3 Hz,
228 1H), 6.08 (d, *J* = 9.4 Hz, 1H), 6.83 (d, *J* = 8.4 Hz, 1H), 7.36 (d, *J* = 9.4 Hz, 1H), 7.93 (m, 6H),
229 8.87 (m, 6H). ¹³C NMR (125 MHz, CDCl₃, 300 K): δ (ppm) 161.25, 156.62, 155.03, 151.61,
230 143.30, 131.07, 130.22, 128.29, 122.48, 116.31, 113.35, 113.11, 106.41, 77.41, 77.16, 76.91.
231
232
233
234
235
236

237
238
239 HR-MS ESI: m/z 557.1527 $[M+H]^+$ (calcd for $C_{33}H_{18}BN_6O_3^+$: 557.1528). HP-LC analysis:
240 retention time 5.68 min.
241
242
243
244

245 2.3.4. Synthesis of compound **5**

246 To a solution of ethynylpyrene (100 mg, 0.44 mmol) in THF (4 mL) was added
247 phenylmagnesium bromide (0.33 mL, 1.0 M), then the solution was stirred for 1 hour at 60°C.
248 Then, a solution of compound **1** (95 mg, 0.22 mmol) in THF (4 mL) was added to the reaction
249 mixture. After heating at 60°C for 16h, the solvent was removed under reduced pressure and
250 the crude product was purified by silica gel column chromatography (eluent: DCM) to afford
251 compound **5** (60 mg, 44%). 1H NMR (500 MHz, $CDCl_3$, 300 K): δ (ppm) 7.41 (d, $J = 8.1$ Hz,
252 1H), 7.60 (d, $J = 9.1$ Hz, 1H), 7.73 (d, $J = 8.2$ Hz, 1H), 7.81 (d, $J = 8.9$ Hz, 1H), 7.85 – 7.90
253 (m, 3H), 7.93 (m, 6H), 8.04 (ddd, $J = 8.3, 5.2, 1.2$ Hz, 2H), 8.92 (m, 6H). ^{13}C NMR (125 MHz,
254 $CDCl_3$, 300 K): δ (ppm) 117.13, 122.32, 124.08, 124.14, 125.35, 125.36, 125.51, 126.09,
255 127.16, 127.97, 128.05, 129.61, 129.86, 130.93, 130.99, 131.12, 131.15, 131.67, 150.70. HR-
256 MS ESI: m/z 621.1980 $[M+H]^+$ (calcd for $C_{42}H_{22}BN_6^+$: 621.1994). HP-LC analysis: retention
257 time 7.84 min.
258
259
260
261
262

263 3. Results and discussion

264
265
266 The synthetic pathway to get new SubPc species **3**, **4**, **5** and **6** is described in Figure 1. The first
267 step was the synthesis of compound **1** following a standard cyclotrimerization reaction of
268 phthalonitrile around a Boron atom[16]. The 1H NMR spectrum of this compound shows two
269 signals, as the form of multiplets lying at 7.95 ppm and 8.90 ppm, that correspond to SubPc-
270 $H\beta$ and SubPc- $H\alpha$ protons, respectively (Fig. S1-1). The low solubility of compound **1** in
271 common organic solvents did not allow us to get a ^{13}C NMR spectrum. Compound **2** was
272 obtained upon reduction of 1-pyrenecarboxaldehyde with $NaBH_4$. The formation of the desired
273 product was confirmed by the emergence of a signal at 5.40 ppm in the 1H NMR spectrum,
274 which corresponds to $-OCH_2-$ protons (Fig. S1-2).
275
276
277

278 SubPc Species **3**, **4** and **6** were successfully synthesized by reacting the antenna with SubPc **1**
279 without addition of a base. Target compounds **3**, **4** and **6** were identified by 1H -NMR and ^{13}C -
280 NMR and by HRMS spectrometry. X-Rays diffraction of SubPc **4** and **6** were also performed,
281 as shown in Figure 2. Judging from these structures, the conic shape of SubPc unit appears to
282 be easily noticeable. The bonds angle between boron, oxygen and carbon atoms slightly
283 changes from 117° in SubPc **4** to 126° in SubPc **6**. It appears that, in the same conditions of
284 temperature and concentration, the antenna **2** took five days to achieve quantitative substitution
285 of the axial chlorine atom in **1**, while the reaction was completed in two days for the others
286 antenna. The lowest reactivity of aliphatic alcohols, compared to phenolic substrates, might be
287 the reason for such a difference in reaction time.
288
289
290
291
292
293
294
295

296
297
298 The synthesis of SubPc **5** was achieved using phenylmagnesium bromide as a base[17] on
299 acidic 1-ethynylpyrene to afford the corresponding ylide that was subsequently reacted with
300 SubPc **1**.
301

302 As an example, the ¹H NMR spectrum of compound **6** is depicted in Figure 3. As mentioned
303 before, signals showing up at 7.92 ppm and at 8.87 ppm correspond to the protons of the SubPc
304 unit. The two doublets with a 9.4 Hz coupling constant, lying at 7.36 ppm and at 6.08 ppm,
305 correspond to the -CH=CH- protons sitting next to the lactone function of the coumarine. The
306 three remaining signals, lying at 5.27 ppm, 5.33 ppm and 6.83 ppm correspond to the benzylic
307 protons of the coumarine unit. The 2.2 Hz coupling constant is associated with the protons from
308 either side of the ether function.
309

310 Signal assignment in the ¹H NMR spectra of compounds **3**, **4** and **5** were more complicated to
311 achieve, due to the presence of multiple overlaid aromatic signals (Fig. S1-4, 6, 8).
312
313

314 315 **4. Photophysical properties**

316 317 *4.1. Photophysical properties*

318
319
320 Absorption and fluorescence properties of subphthalocyanines **1**, **3-6** were studied by UV-
321 Visible spectroscopy and are gathered in Table 1. The absorption and emission spectra of
322 compound **1**, **3-6** were recorded in toluene, tetrahydrofuran, chloroform, dimethyl sulfoxide
323 and methanol, from an aprotic apolar to a protic polar solvent. Although highest values of
324 absorption/emission maxima were obtained when the compounds were in solution in DMSO,
325 no solvatochromism was noticeable. Also, no aggregation was observed on spectra, due to the
326 three-dimensional design of molecules.
327

328 All compounds possess maximum absorption wavelengths between 560 and 572 nm
329 (subphthalocyanine partner) and UV-blue absorption bands between 250 and 370 nm (pyrene
330 or coumarine partners) (Figure 4). Associated maximum emission wavelengths were measured
331 with a Stokes shift around 10 nm. Introduction of the pyrenyl antenna linked to a triple bond in
332 subphthalocyanine **5** seems to red-shift both absorption and emission maxima by ca. 5 nm. The
333 observation of distinct absorbance peaks with no (or small) shifts in the absorption values
334 indicate that chromophores do not interact between each other.
335

336 Functionalization of the boron atom with aryloxy/alkoxy moieties upon substitution of the
337 chlorine atom lowers the fluorescence quantum yield of the molecule by a factor 2, resulting in
338 compounds with fluorescence quantum yields ranging from 0.11 to 0.25, depending on the
339 solvent (highest values are obtained for aprotic apolar solvents), except for subphthalocyanine
340 **4**, which did not appear to fluoresce.
341
342

343 344 *4.2. Energy transfer studies*

355
356
357 Energy transfer properties of antenna-subphthalocyanine conjugates were investigated by
358 fluorescence spectroscopy and are gathered in Table 1. The fluorescence emission spectra of
359 compounds **3-6** were investigated using an excitation wavelength of 345 nm for compounds **3**
360 and **4**, 360 nm for compound **5** and 305 nm for compound **6**, at 25°C in various solvents (Fig.
361 S5-1, 2). Unfortunately, no energy transfer between the pyrenyl unit and the subphthalocyanine
362 platform seems to occur in compound **4**. Also, even if any residual fluorescence of the
363 coumarine unit could not be observed upon excitation at the antenna and subsequent energy
364 transfer in compound **6** (corresponding to an efficient energy transfer), it was not possible to
365 determine the energy transfer efficiency (E.T.E.) due to the absorption wavelength of the
366 antenna, located right in the absorption of the subphthalocyanine. On the other hand,
367 compounds **3** and **5** did show efficient energy transfer processes, ranging from 36% to 84% in
368 **3** and from 84% to 96% in **5**. In both cases, a strong emission peak around 575 nm was observed
369 upon excitation in the UV-blue region of the spectrum, with residual fluorescence of the pyrenyl
370 antenna for compound **3**. The high E.T.E. values obtained with compound **5** does indicate a
371 really good energy transfer process between the pyrenyl unit linked to the subphthalocyanine
372 platform through a triple bond. At this stage t whether the energy transfer takes place through
373 the triple bond or through space is a question left opened.
374
375
376
377
378
379
380

381 **5. Conclusion**

382
383
384 This work showed that the introduction of antenna at the axial position of subphthalocyanine **1**
385 was successfully performed whatever the nature of the linker. These new conjugates were fully
386 characterized by ¹H-NMR and ¹³C-NMR, mass spectrometry, UV-Vis, fluorescence and X-ray
387 diffraction for compounds **4** and **6**. Absorption and emission measurements showed that an
388 efficient energy transfer occurred in compounds **3**, **5** and **6**, with E.T.E. values reaching 95%
389 for compound **5**. These new dyads appeared as promising molecular constructs used for
390 applications requiring such energy transfers, such as photovoltaics, molecular probes.
391
392
393
394

395 **Acknowledgment**

396 We acknowledge Canceropôle Est and FEDER for Funding (RD) and the French Ministry of
397 Higher Education, Research and Innovation for a fellowship (VL). PACSMUB platform is
398 acknowledged for allowing access to all spectrometers to perform the analyses (NMR, Mass).
399 Dr Kévin Renault is acknowledged for discussion and advices regarding fluorescence studies.
400
401
402

403 **References**

- 404
405 [1] Balzani V, Credi A, Venturi M. Photochemical conversion of solar energy. *ChemSusChem*.
406 2008;1(1-2):26-58.
407 [2] Shrestha D, Jenei A, Nagy P, Vereb G, Szollosi J. Understanding FRET as a research tool
408 for cellular studies. *Int J Mol Sci*. 2015;16(4):6718-56.
409
410
411
412
413

- 414
415
416 [3] Rowland CE, Brown CW, Medintz IL, Delehanty JB. Intracellular FRET-based probes: a
417 review. *Methods Appl Fluoresc.* 2015;3(4):042006.
418 [4] Chitta R, Sandanayaka ASD, Schumacher AL, D'Souza L, Araki Y, Ito O, et al. Donor-
419 Acceptor Nanohybrids of Zinc Naphthalocyanine or Zinc Porphyrin Noncovalently
420 Linked to Single-Wall Carbon Nanotubes for Photoinduced Electron Transfer. *J Phys Chem.*
421 2007;111:6947-55.
422 [5] Lazarides T, Charalambidis G, Vuillamy A, Reglier M, Klontzas E, Froudakis G, et al.
423 Promising fast energy transfer system via an easy synthesis: Bodipy-porphyrin dyads connected
424 via a cyanuric chloride bridge, their synthesis, and electrochemical and photophysical
425 investigations. *Inorg Chem.* 2011;50(18):8926-36.
426 [6] Bizet F, Ipuay M, Bernhard Y, Lioret V, Winckler P, Goze C, et al. Cellular imaging using
427 BODIPY-, pyrene- and phthalocyanine-based conjugates. *Bioorg Med Chem.* 2018;26(2):413-
428 20.
429 [7] Klaus D, Knecht R, DragÄsser A, Keil C, Schlettwein D. (Photo-)conduction
430 measurements during the growth of evaporated bulk heterojunctions of a subphthalocyanine
431 donor and a perfluorinated phthalocyanine acceptor. *physica status solidi (a).* 2009:NA-NA.
432 [8] Winckel E, Mascaraque M, Zamarr3n A, Juarranz de la Fuente 3, Torres T, Escosura A.
433 Dual Role of Subphthalocyanine Dyes for Optical Imaging and Therapy of Cancer. *Advanced*
434 *Functional Materials.* 2018;28(24):1705938.
435 [9] Del Rey B, Keller U, Torres T, Rojo G, Agullo-Lopez F, Nonell S, et al. Synthesis and
436 Nonlinear Optical, Photophysical, and Electrochemical
437 Properties of Subphthalocyanines. *J Am Chem Soc.* 1998;120:12808-17.
438 [10] Martin G, Rojo G, Agullo-Lopez F, Ferro VR, Garcia de la Vega JM, Martinez-Diaz MV,
439 et al. Subphthalocyanines and Subnaphthalocyanines: Nonlinear Quasi-Planar Octupolar
440 Systems with Permanent Polarity. *J phys Chem B.* 2002;106:13139-45.
441 [11] a) El-Khouly ME, El-Refaey A, Nam W, Fukuzumi S, Goktug O, Durmus M. A
442 subphthalocyanine-pyrene dyad: electron transfer and singlet oxygen generation. *Photochem*
443 *Photobiol Sci.* 2017;16(10):1512-8; b) Gotfredsen H, Kilde MD, Santella M, Kadziola A,
444 Nielsen MB. Fluorescence switching with subphthalocyanine- dihydroazulene dyads. *Mol.*
445 *Syst. Des. Eng.,* 2019, (4): 199-205.
446 [12] Claessens Christian G, Gonz3lez-Rodr3guez D, del Rey B, Torres T, Mark G, Schuchmann
447 H-P, et al. Highly Efficient Synthesis of Chloro- and Phenoxy-Substituted Subphthalocyanines.
448 *European Journal of Organic Chemistry.* 2003;2003(14):2547-51.
449 [13] Ziessel R, Ulrich G, Elliott KJ, Harriman A. Electronic energy transfer in molecular dyads
450 built around boron-ethyne-substituted subphthalocyanines. *Chemistry.* 2009;15(20):4980-4.
451 [14] Xu H, Ng DK. Preparation, spectroscopic properties, and stability of water-soluble
452 subphthalocyanines. *Chem Asian J.* 2009;4(1):104-10.
453 [15] Bernhard Y, Winckler P, Chassagnon R, Richard P, Gigot E, Perrier-Cornet JM, et al.
454 Subphthalocyanines: addressing water-solubility, nano-encapsulation, and activation for
455 optical imaging of B16 melanoma cells. *Chem Commun (Camb).* 2014;50(90):13975-8.
456 [16] Morse GE, Paton AS, Lough A, Bender TP. Chloro boron subphthalocyanine and its
457 derivatives: dyes, pigments or somewhere in between? *Dalton Trans.* 2010;39(16):3915-22.
458 [17] Camerel F, Ulrich G, Retailleau P, Ziessel R. Ethynyl-boron subphthalocyanines
459 displaying efficient cascade energy transfer and large Stokes shifts. *Angew Chem Int Ed Engl.*
460 2008;47(46):8876-80.
461
462
463
464
465
466
467
468
469
470
471
472

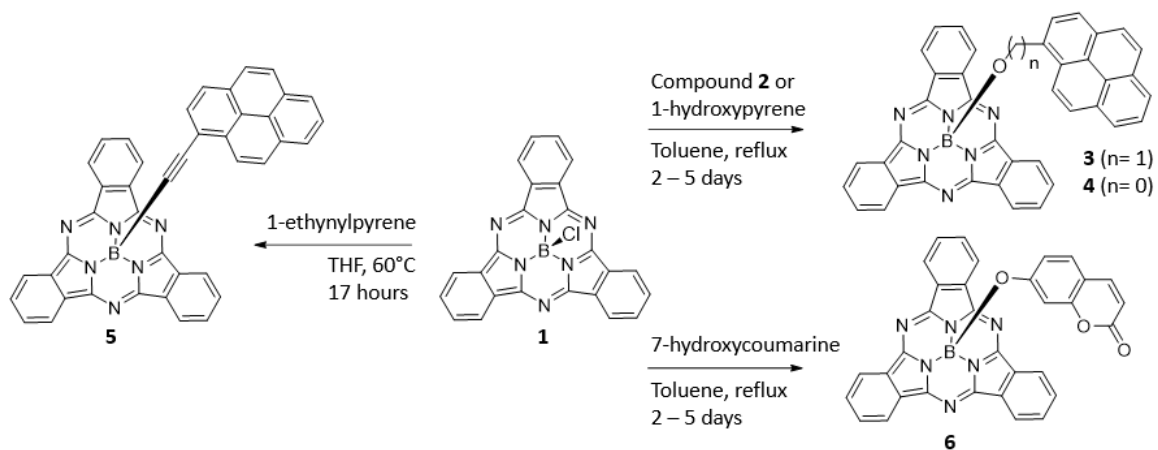


Figure 1: Synthetic pathway to compounds **3**, **4**, **5** and **6**

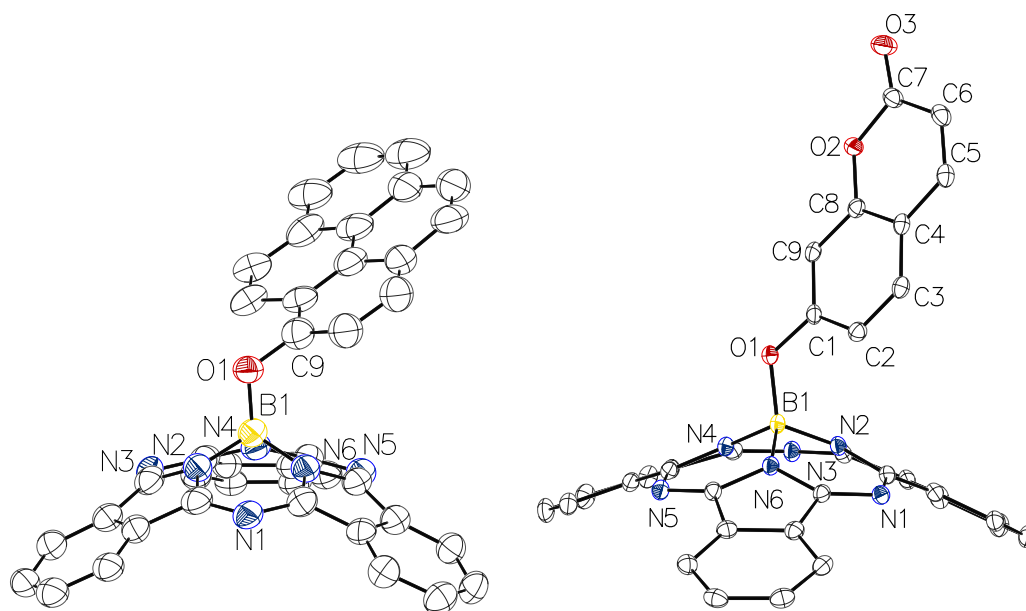
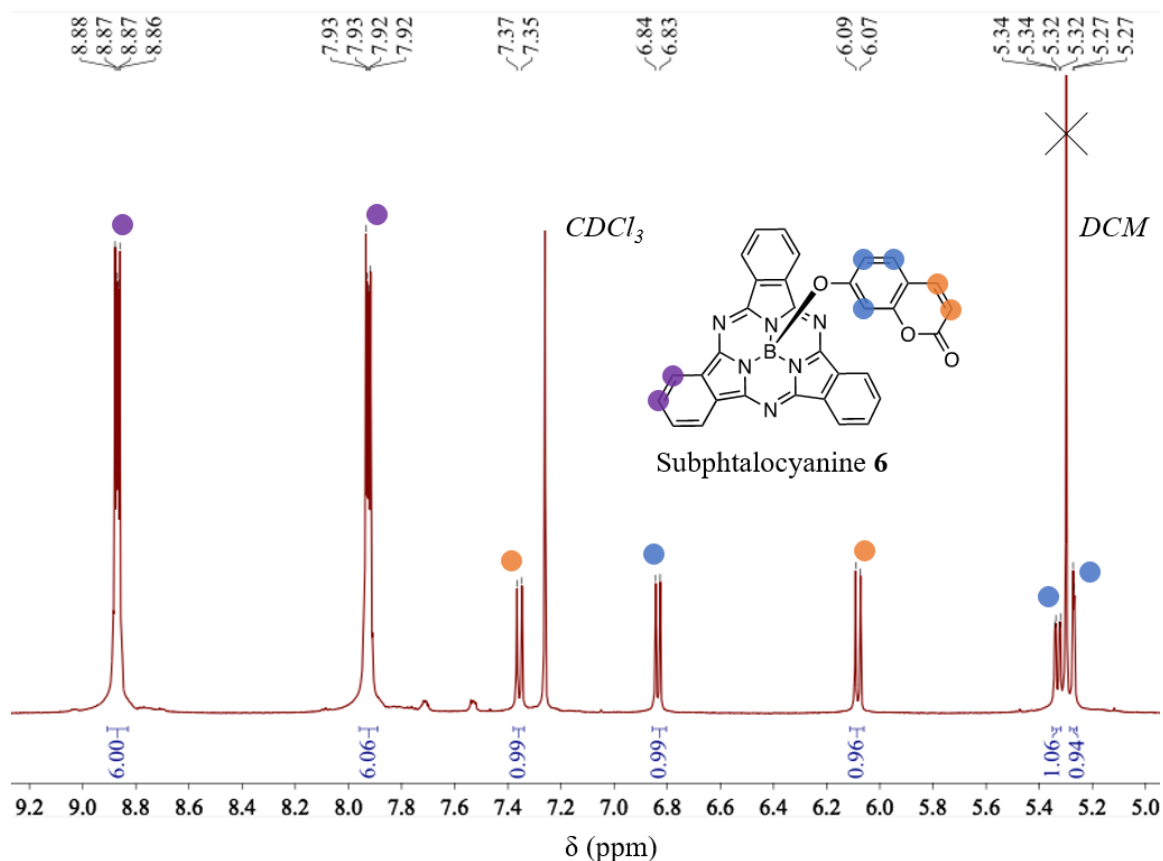


Figure 2: ORTEP view of compounds **4** (left) and **6** (right). Thermal ellipsoids are drawn at 50 % probability plot.



559
560
561
562
563
564

565
566
567
568
569
570
571
572
573
574
575
576
577
578
579
580
581
582
583
584
585
586
587
588
589
590

Cpd	Solvent	$\lambda_{\text{Abs/Em}}$ (nm)	ϵ (L.mol ⁻¹ .cm ⁻¹)	Q. Y.	E. T. E.
1	Toluene	565/572	63000	0.48	
	THF	562/572	n. d.	0.32	
	CHCl ₃	565/571	67500	0.32	/
	DMSO	569/578	n. d.	0.37	
	MeOH	562/572	n. d.	0.27	
3	Toluene	563/574	50900	0.23	n. d.
	THF	560/572	44000	0.18	36%
	CHCl ₃	563/576	46000	0.17	78%
	DMSO	567/578	45000	0.21	84%
	MeOH	562/576	39100	0.13	43%
4	Toluene	563/572	76600	0.01	
	THF	562/574	58600	<0.01	
	CHCl ₃	564/574	78200	<0.01	/
	DMSO	566/576	77700	<0.01	
	MeOH	560/570	66700	<0.01	

	Toluene	568/576	96000	0.20	84%
	EtOAc	564/574	88700	0.16	n. d.
	THF	566/576	70000	0.22	93%
5	CHCl ₃	568/578	90800	0.18	96%
	MeCN	565/576	81100	0.18	n. d.
	DMSO	572/582	84300	0.20	94%
	MeOH	565/576	79300	0.11	95%
	Toluene	564/574	68400	0.25	
	THF	562/572	62000	0.19	
6	CHCl ₃	564/574	65000	0.19	/
	DMSO	567/578	66600	0.23	
	MeOH	561/574	59200	0.17	

Table 1: spectroscopic properties of synthesized subphthalocyanines

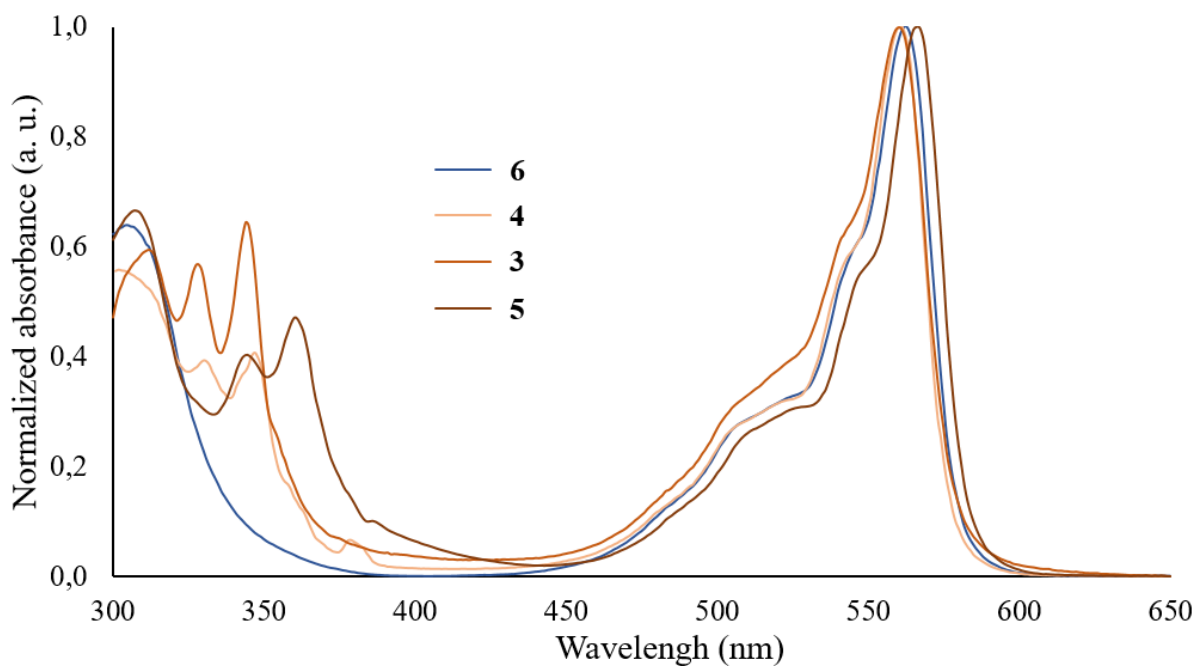


Figure 4: Absorption spectra of compounds **3**, **4**, **5** and **6** measured in THF

checkCIF/PLATON report

You have not supplied any structure factors. As a result the full set of tests cannot be run.

THIS REPORT IS FOR GUIDANCE ONLY. IF USED AS PART OF A REVIEW PROCEDURE FOR PUBLICATION, IT SHOULD NOT REPLACE THE EXPERTISE OF AN EXPERIENCED CRYSTALLOGRAPHIC REFEREE.

No syntax errors found. CIF dictionary Interpreting this report

Datablock: compound_4

Bond precision: C-C = 0.0091 A Wavelength=1.54178

Cell: a=9.9592(4) b=12.1772(5) c=13.5700(6)
 alpha=113.192(2) beta=96.701(3) gamma=103.825(2)

Temperature: 100 K

	Calculated	Reported
Volume	1427.34(11)	1427.34(11)
Space group	P -1	P -1
Hall group	-P 1	-P 1
Moiety formula	C40 H21 B N6 O	C40 H21 B N6 O
Sum formula	C40 H21 B N6 O	C40 H21 B N6 O
Mr	612.44	612.44
Dx,g cm-3	1.425	1.425
Z	2	2
Mu (mm-1)	0.700	0.700
F000	632.0	632.0
F000'	633.80	
h,k,lmax	11,14,16	11,14,16
Nref	5090	5023
Tmin,Tmax	0.922,0.957	0.733,0.915
Tmin'	0.783	

Correction method= # Reported T Limits: Tmin=0.733 Tmax=0.915
AbsCorr = MULTI-SCAN

Data completeness= 0.987 Theta(max)= 66.941

R(reflections)= 0.1041(3266) wR2(reflections)= 0.2813(5023)

S = 1.048 Npar= 433

The following ALERTS were generated. Each ALERT has the format

test-name_ALERT_alert-type_alert-level.

Click on the hyperlinks for more details of the test.

● **Alert level C**

PLAT084_ALERT_3_C	High wR2 Value (i.e. > 0.25)	0.28	Report
PLAT230_ALERT_2_C	Hirshfeld Test Diff for C21	--C24 .	6.2	s.u.
PLAT234_ALERT_4_C	Large Hirshfeld Difference C15	--C16 .	0.18	Ang.
PLAT234_ALERT_4_C	Large Hirshfeld Difference C16	--C17 .	0.18	Ang.
PLAT340_ALERT_3_C	Low Bond Precision on C-C Bonds	0.00914	Ang.

● **Alert level G**

PLAT012_ALERT_1_G	No _shelx_res_checksum Found in CIF	Please	Check
PLAT072_ALERT_2_G	SHELXL First Parameter in WGHT	Unusually Large	0.12	Report
PLAT335_ALERT_2_G	Check Large C6 Ring C-C Range	C12 -C15	0.17	Ang.
PLAT432_ALERT_2_G	Short Inter X...Y Contact C6B	..C6B	3.19	Ang.
	1-x,1-y,-z =	2_665	Check	

- 0 **ALERT level A** = Most likely a serious problem - resolve or explain
0 **ALERT level B** = A potentially serious problem, consider carefully
5 **ALERT level C** = Check. Ensure it is not caused by an omission or oversight
4 **ALERT level G** = General information/check it is not something unexpected
- 1 ALERT type 1 CIF construction/syntax error, inconsistent or missing data
4 ALERT type 2 Indicator that the structure model may be wrong or deficient
2 ALERT type 3 Indicator that the structure quality may be low
2 ALERT type 4 Improvement, methodology, query or suggestion
0 ALERT type 5 Informative message, check
-

Datablock: compound_6

Bond precision:	C-C = 0.0025 A	Wavelength=1.54178	
Cell:	a=11.2700(6)	b=16.3338(9)	c=15.6723(6)
	alpha=90	beta=101.100(3)	gamma=90
Temperature:	100 K		
	Calculated	Reported	
Volume	2831.0(2)	2831.0(2)	
Space group	P 21/c	P 1 21/c 1	
Hall group	-P 2ybc	-P 2ybc	
Moiety formula	C33 H17 B N6 O3, C H2 Cl2	C33 H17 B N6 O3, C H2 Cl2	
Sum formula	C34 H19 B Cl2 N6 O3	C34 H19 B Cl2 N6 O3	
Mr	641.26	641.26	
Dx,g cm-3	1.505	1.505	
Z	4	4	
Mu (mm-1)	2.478	2.478	
F000	1312.0	1312.0	
F000'	1318.52		
h,k,lmax	13,19,18	13,19,18	
Nref	5029	5018	
Tmin,Tmax	0.520,0.788	0.447,0.621	
Tmin'	0.276		


Correction method= # Reported T Limits: Tmin=0.447 Tmax=0.621
AbsCorr = MULTI-SCAN

Data completeness= 0.998 Theta(max)= 66.797

R(reflections)= 0.0354(4461) wR2(reflections)= 0.0895(5018)

S = 1.069 Npar= 415

The following ALERTS were generated. Each ALERT has the format
test-name_ALERT_alert-type_alert-level.
Click on the hyperlinks for more details of the test.

 **Alert level G**

PLAT012_ALERT_1_G No _shelx_res_checksum Found in CIF Please Check

-
- 0 **ALERT level A** = Most likely a serious problem - resolve or explain
 - 0 **ALERT level B** = A potentially serious problem, consider carefully
 - 0 **ALERT level C** = Check. Ensure it is not caused by an omission or oversight
 - 1 **ALERT level G** = General information/check it is not something unexpected
-
- 1 ALERT type 1 CIF construction/syntax error, inconsistent or missing data
 - 0 ALERT type 2 Indicator that the structure model may be wrong or deficient
 - 0 ALERT type 3 Indicator that the structure quality may be low
 - 0 ALERT type 4 Improvement, methodology, query or suggestion
 - 0 ALERT type 5 Informative message, check
-

It is advisable to attempt to resolve as many as possible of the alerts in all categories. Often the minor alerts point to easily fixed oversights, errors and omissions in your CIF or refinement strategy, so attention to these fine details can be worthwhile. In order to resolve some of the more serious problems it may be necessary to carry out additional measurements or structure refinements. However, the purpose of your study may justify the reported deviations and the more serious of these should normally be commented upon in the discussion or experimental section of a paper or in the "special_details" fields of the CIF. checkCIF was carefully designed to identify outliers and unusual parameters, but every test has its limitations and alerts that are not important in a particular case may appear. Conversely, the absence of alerts does not guarantee there are no aspects of the results needing attention. It is up to the individual to critically assess their own results and, if necessary, seek expert advice.

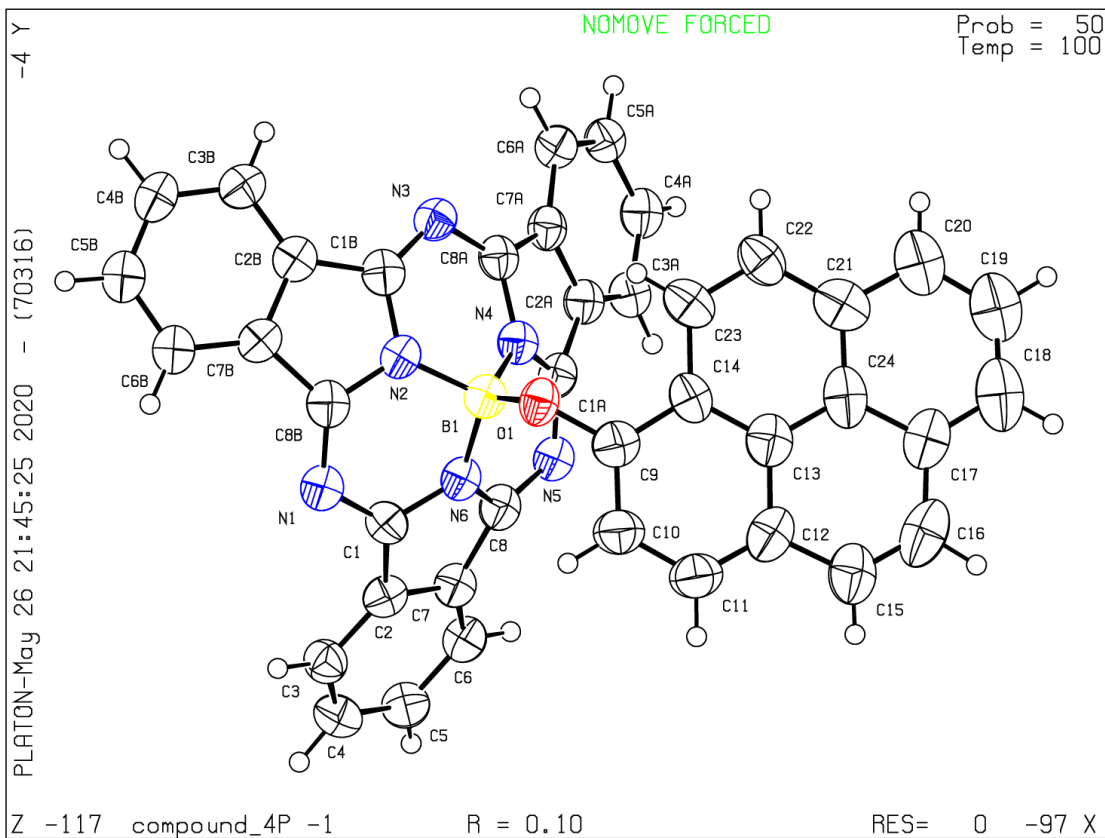
Publication of your CIF in IUCr journals

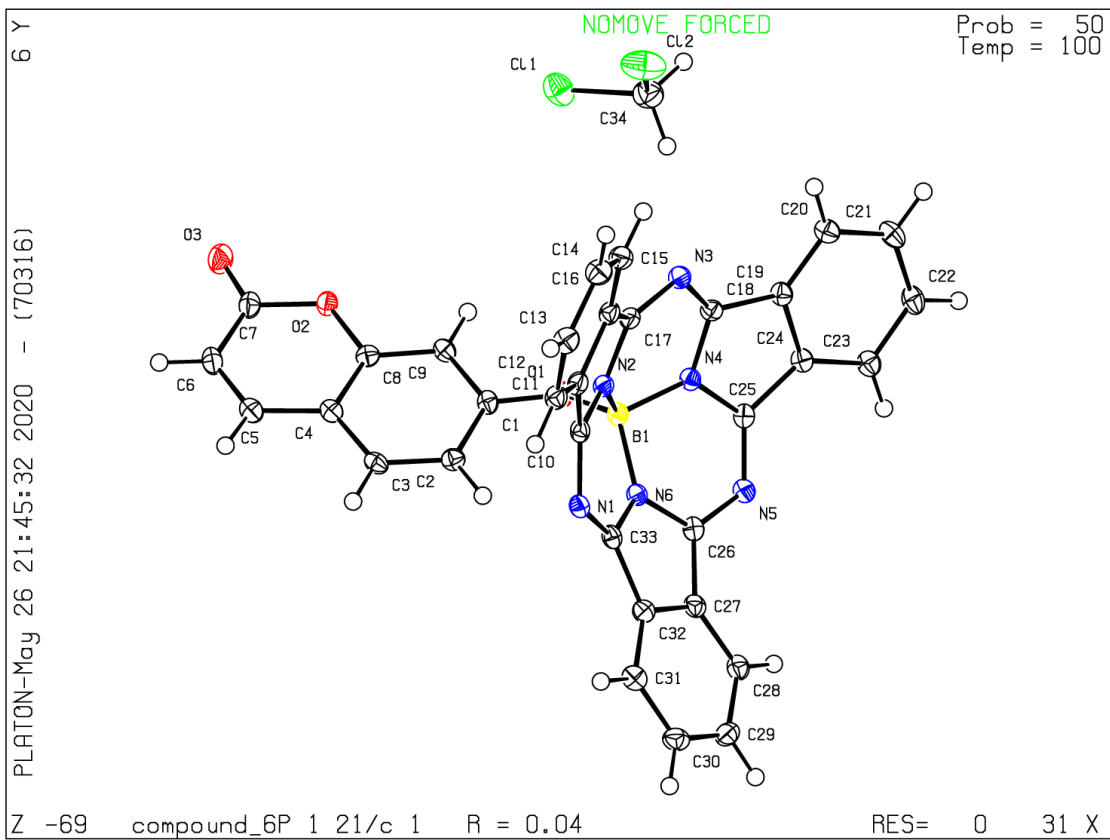
A basic structural check has been run on your CIF. These basic checks will be run on all CIFs submitted for publication in IUCr journals (*Acta Crystallographica*, *Journal of Applied Crystallography*, *Journal of Synchrotron Radiation*); however, if you intend to submit to *Acta Crystallographica Section C* or *E* or *IUCrData*, you should make sure that full publication checks are run on the final version of your CIF prior to submission.

Publication of your CIF in other journals

Please refer to the *Notes for Authors* of the relevant journal for any special instructions relating to CIF submission.

PLATON version of 22/04/2020; check.def file version of 09/03/2020





Declaration of interests

The authors declare that they have no known competing financial interests or personal relationships that could have appeared to influence the work reported in this paper.

The authors declare the following financial interests/personal relationships which may be considered as potential competing interests:

Pyrene/coumarine-subphthalocyanine conjugates as light harvesting systems with intramolecular energy transfer

Vivian Lioret^a, Yoann Rousselin^a, Richard A. Decréau^{a*}

SUPPORTING INFORMATIONS

OUTLINE

I. ¹ H and ¹³ C NMR spectra	S-2
II. RP-HPLC elution profiles of compounds 01 , 03 , 04 , 05 and 06	S-8
III. HRMS analysis	S-11
IV. Absorbance, excitation and emission spectra of compounds 01 , 03 , 04 , 05 and 06 in different solvents	S-14
V. Energy Transfer Efficiency studies of compounds 03 and 05 in different solvents	S-19
VI. X-Ray diffraction informations for compounds 4 and 6	S-21

I. ^1H and ^{13}C NMR spectra

Figure S1-1: ^1H NMR spectrum of compound **01** recorded in CDCl_3 at 500 MHz and 300 K

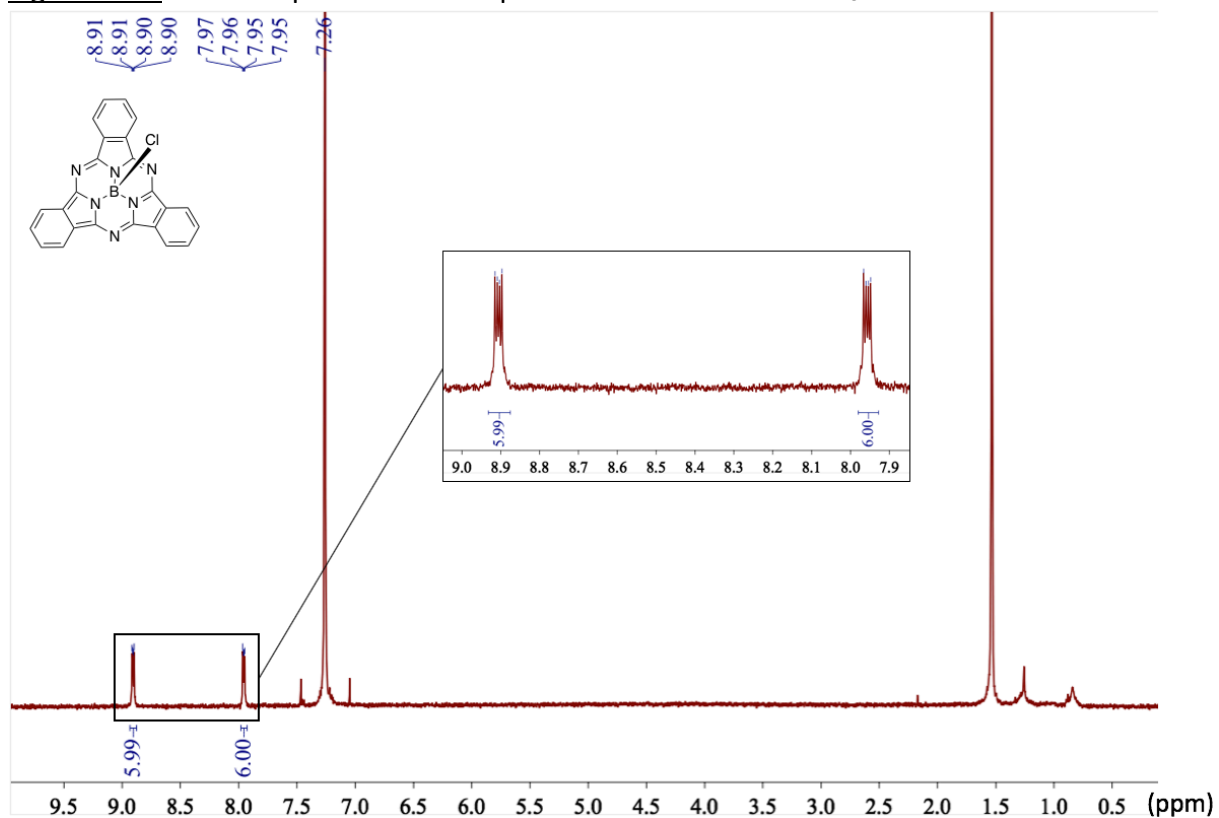


Figure S1-2: ^1H NMR spectrum of compound **02** recorded in CDCl_3 at 500 MHz and 300 K

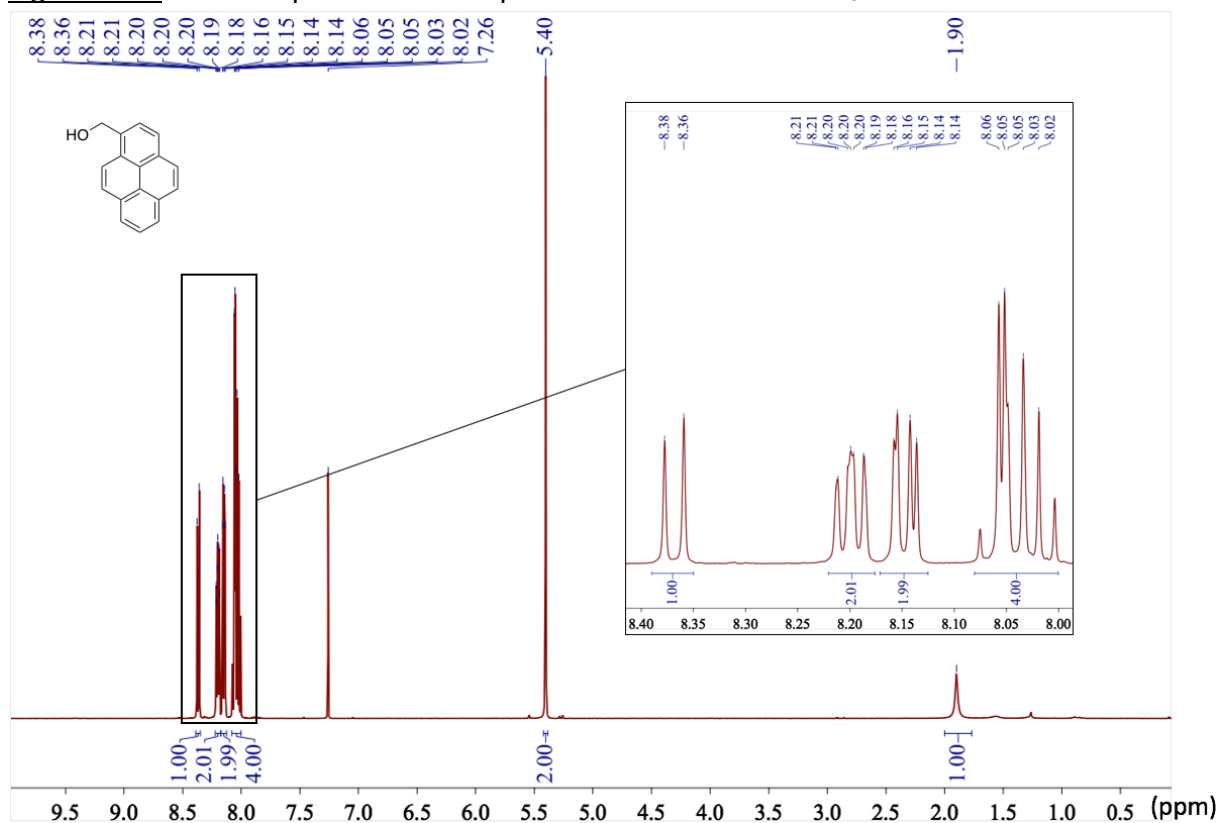


Figure S1-3: ^{13}C NMR spectrum of compound **02** recorded in CDCl_3 at 125 MHz and 300 K

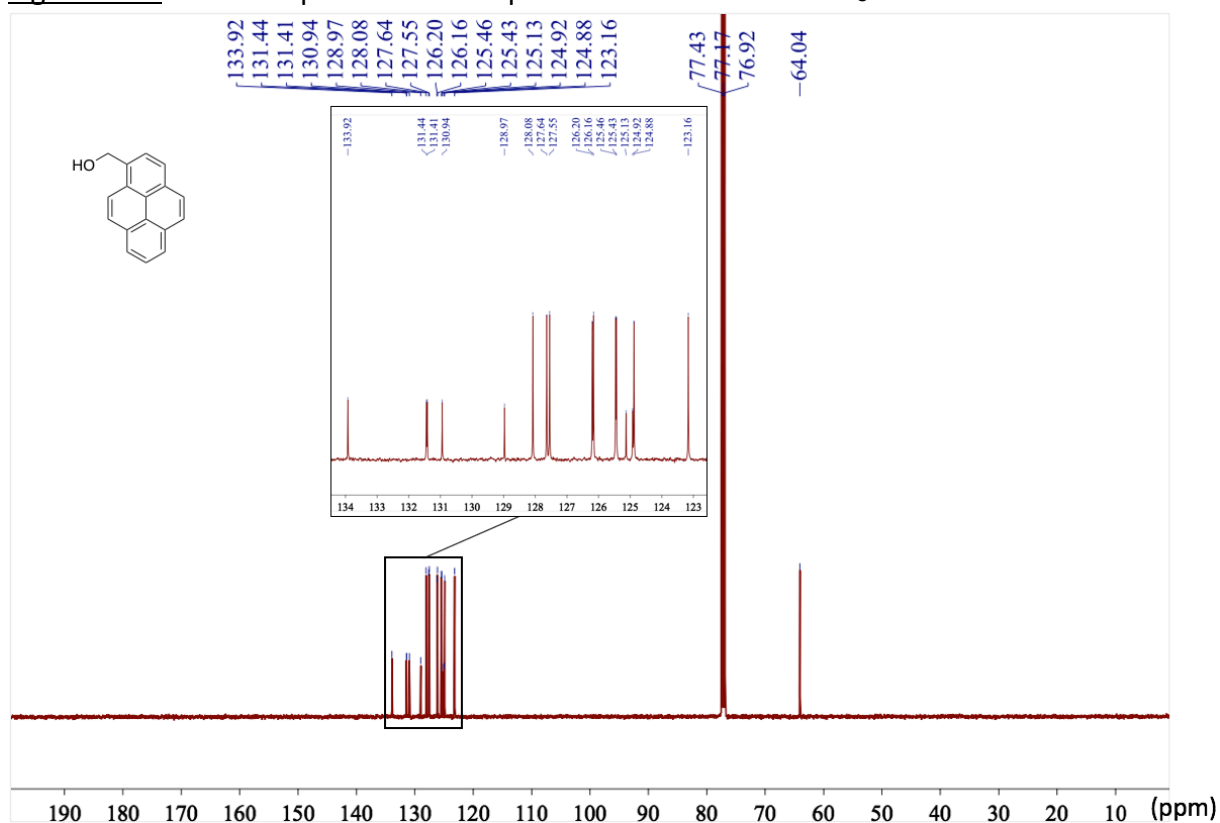


Figure S1-4: ^1H NMR spectrum of compound **03** recorded in CDCl_3 at 500 MHz and 300 K

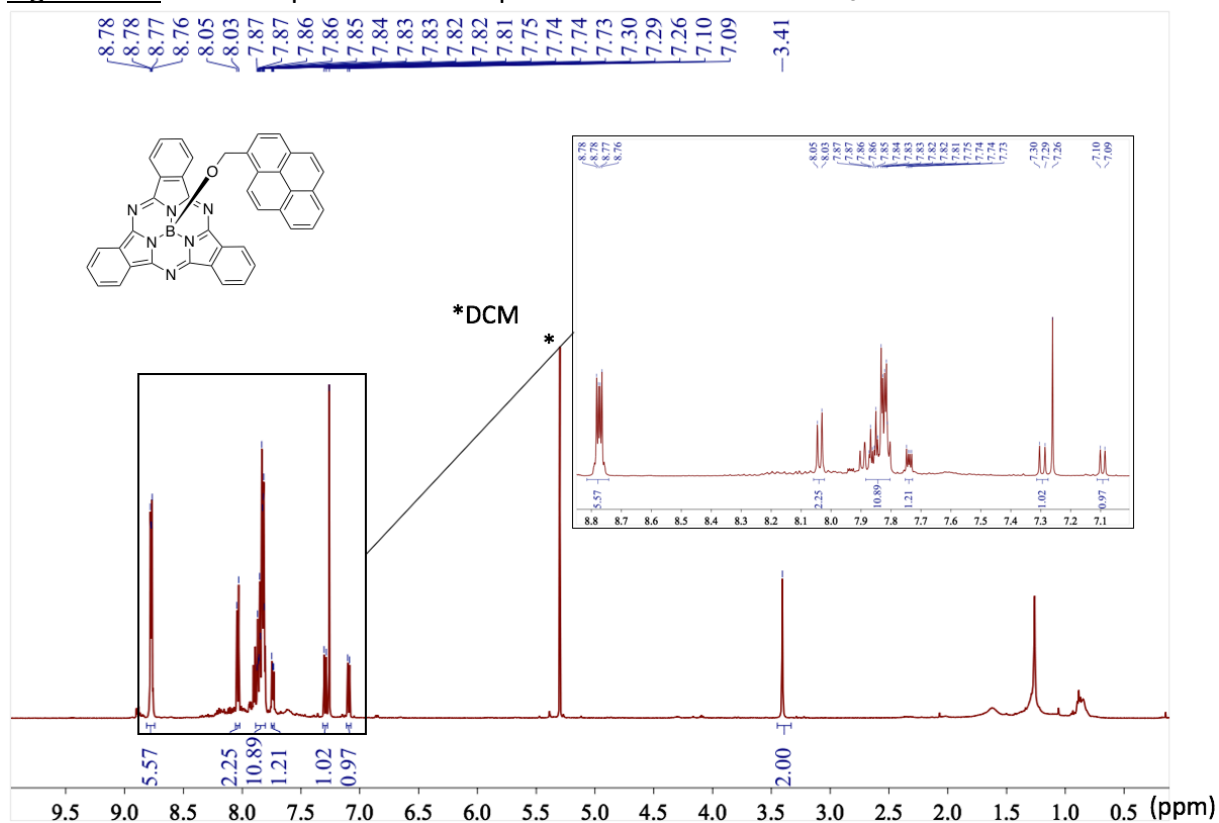


Figure S1-5: ^{13}C NMR spectrum of compound **03** recorded in CDCl_3 at 125 MHz and 300 K

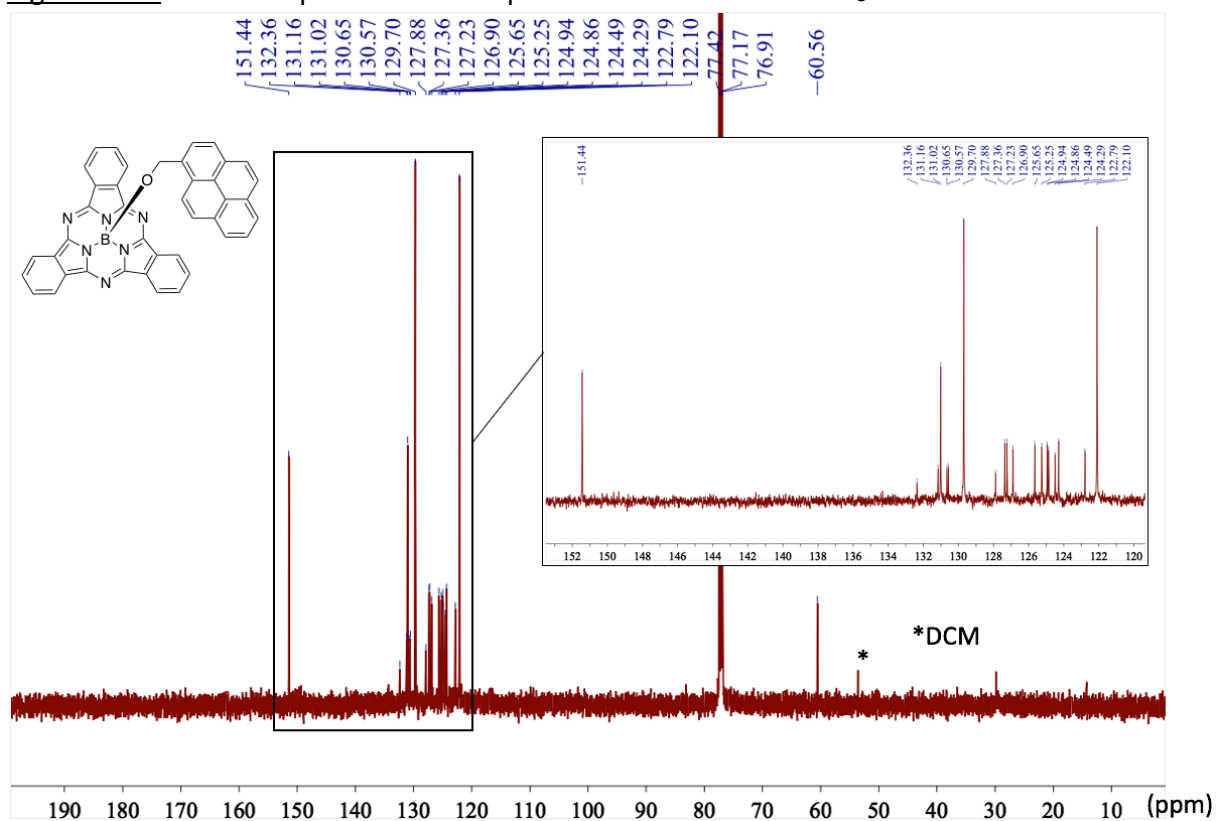


Figure S1-6: ^1H NMR spectrum of compound **04** recorded in CDCl_3 at 500 MHz and 300 K

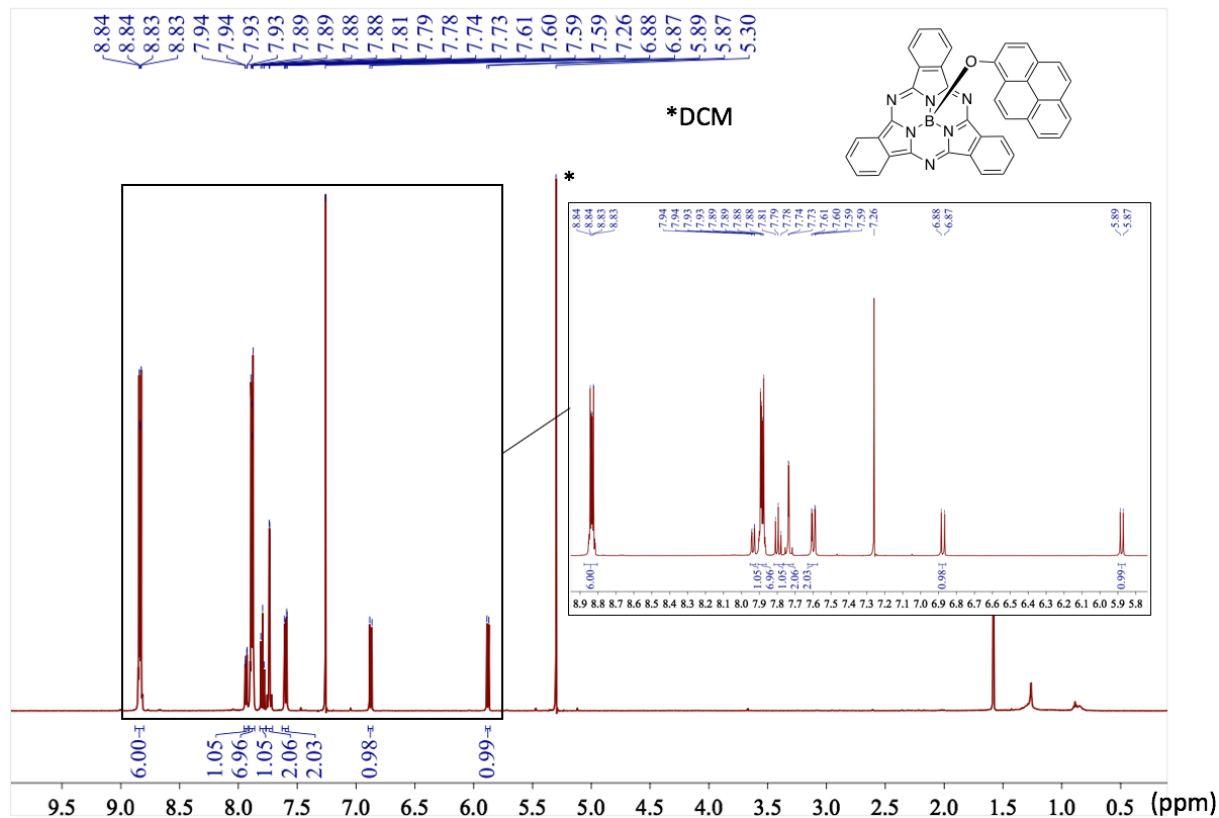


Figure S1-7: ^{13}C NMR spectrum of compound **04** recorded in CDCl_3 at 125 MHz and 300 K

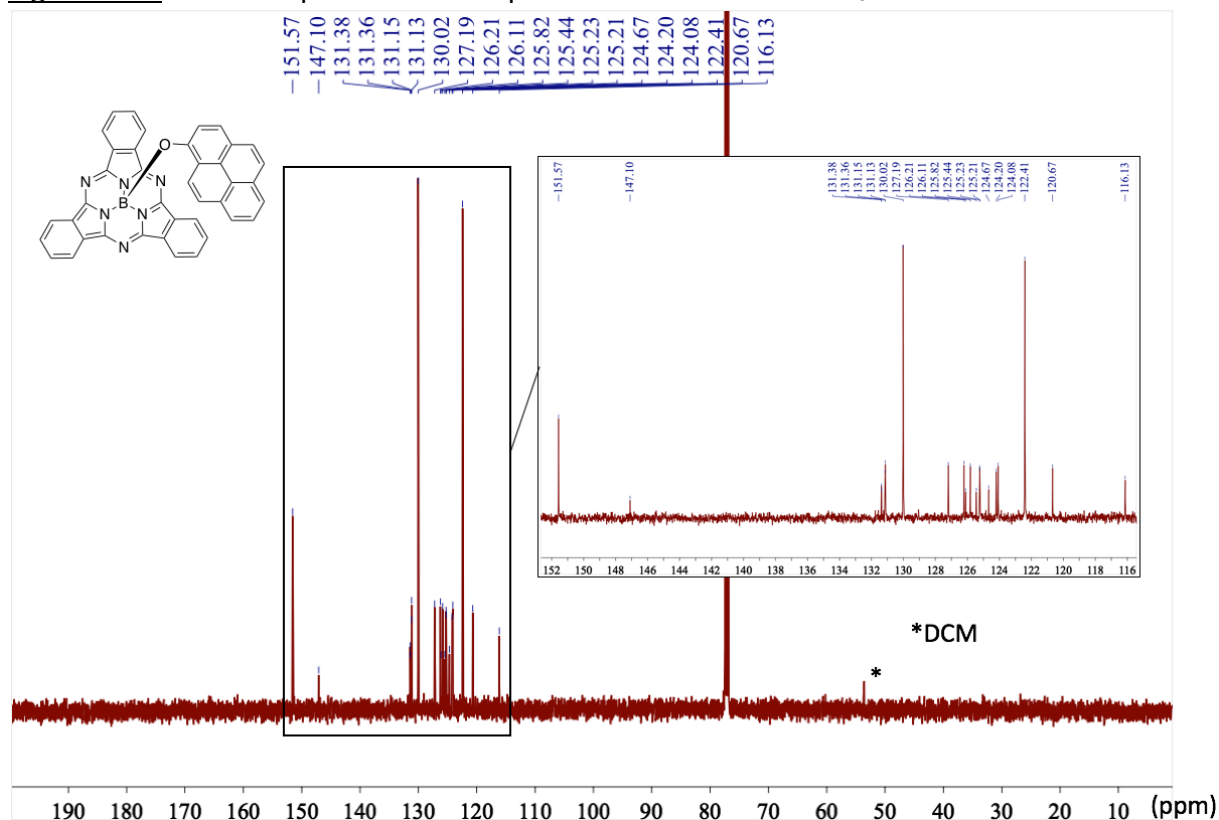


Figure S1-8: ^1H NMR spectrum of compound **05** recorded in CDCl_3 at 500 MHz and 300 K

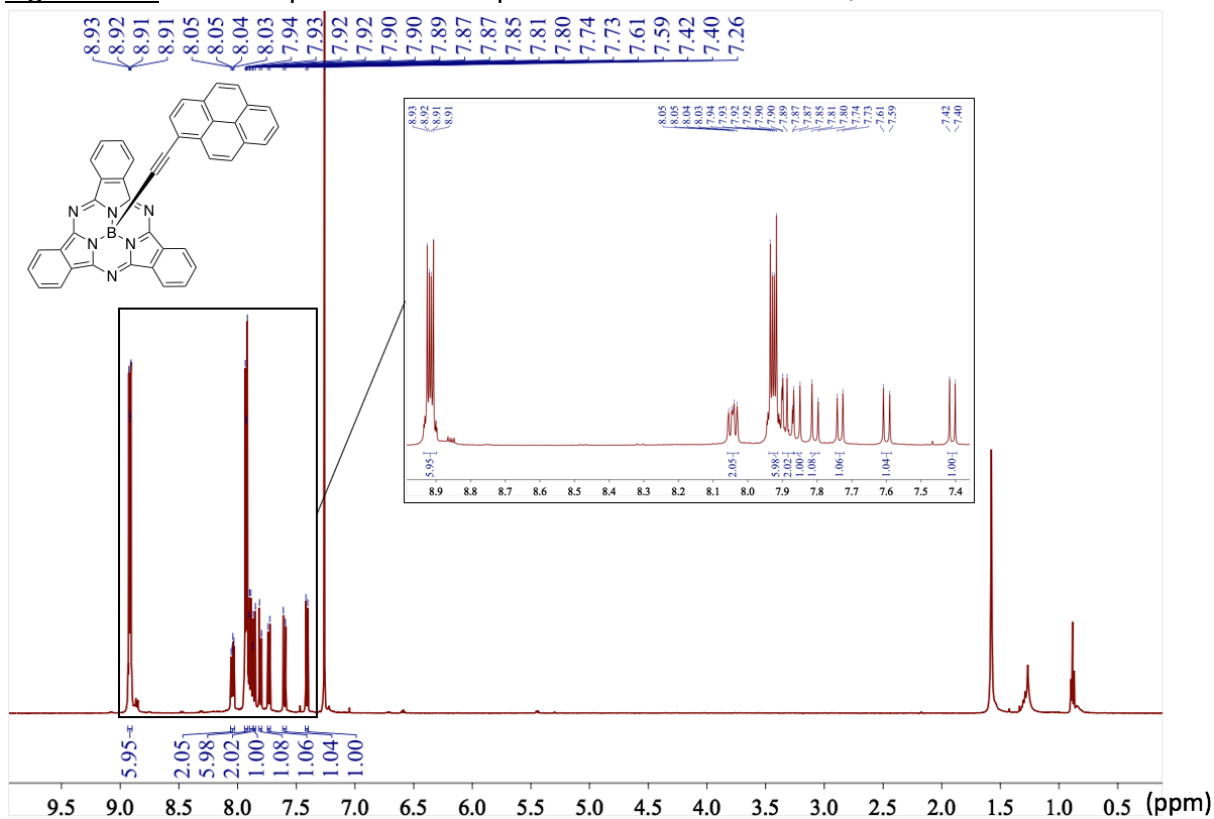


Figure S1-9: ^{13}C NMR spectrum of compound **05** recorded in CDCl_3 at 125 MHz and 300 K

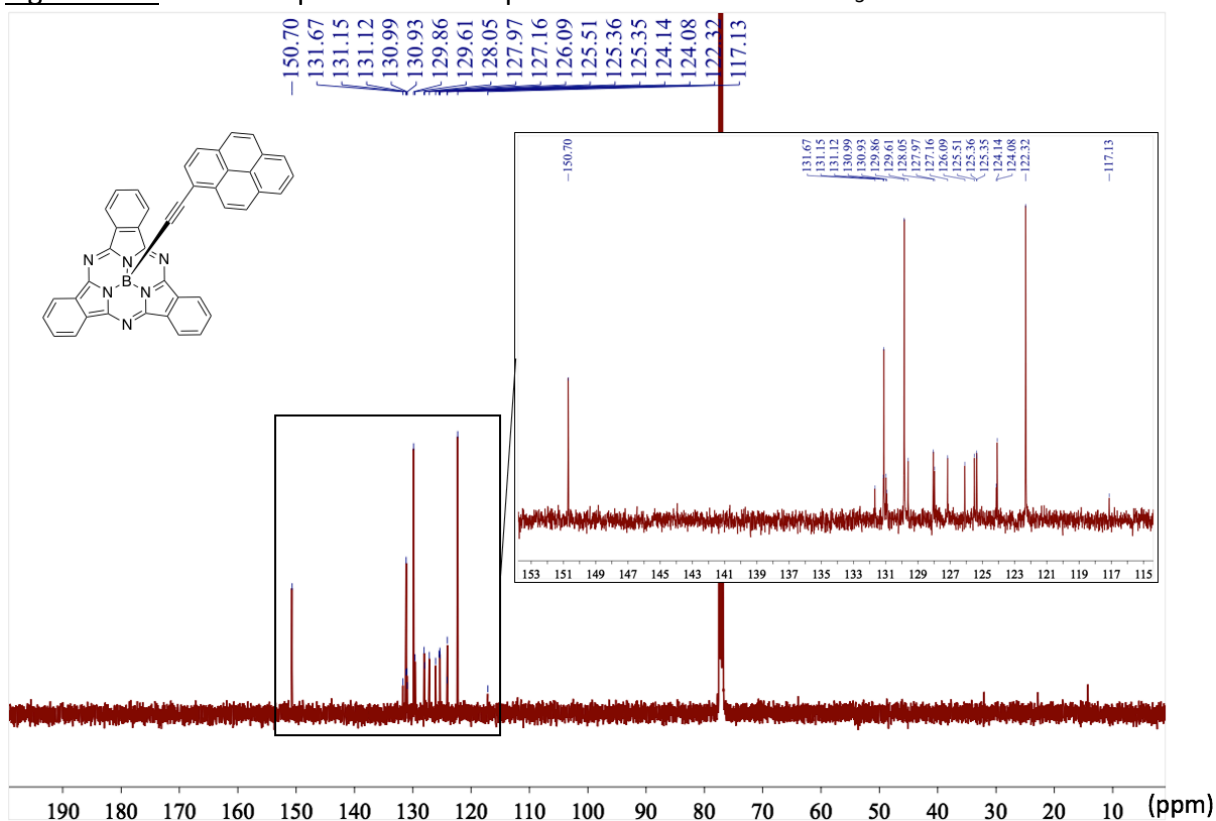


Figure S1-10: ^1H NMR spectrum of compound **06** recorded in CDCl_3 at 500 MHz and 300 K

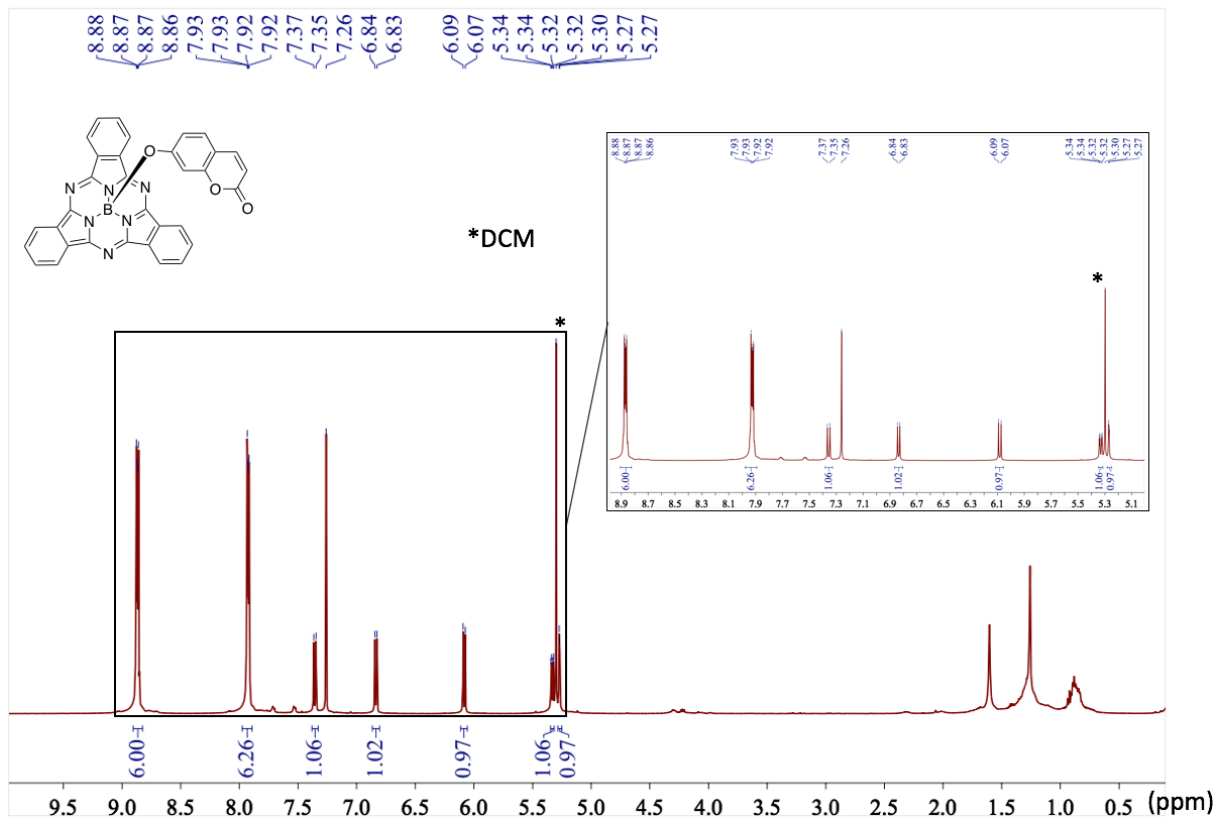
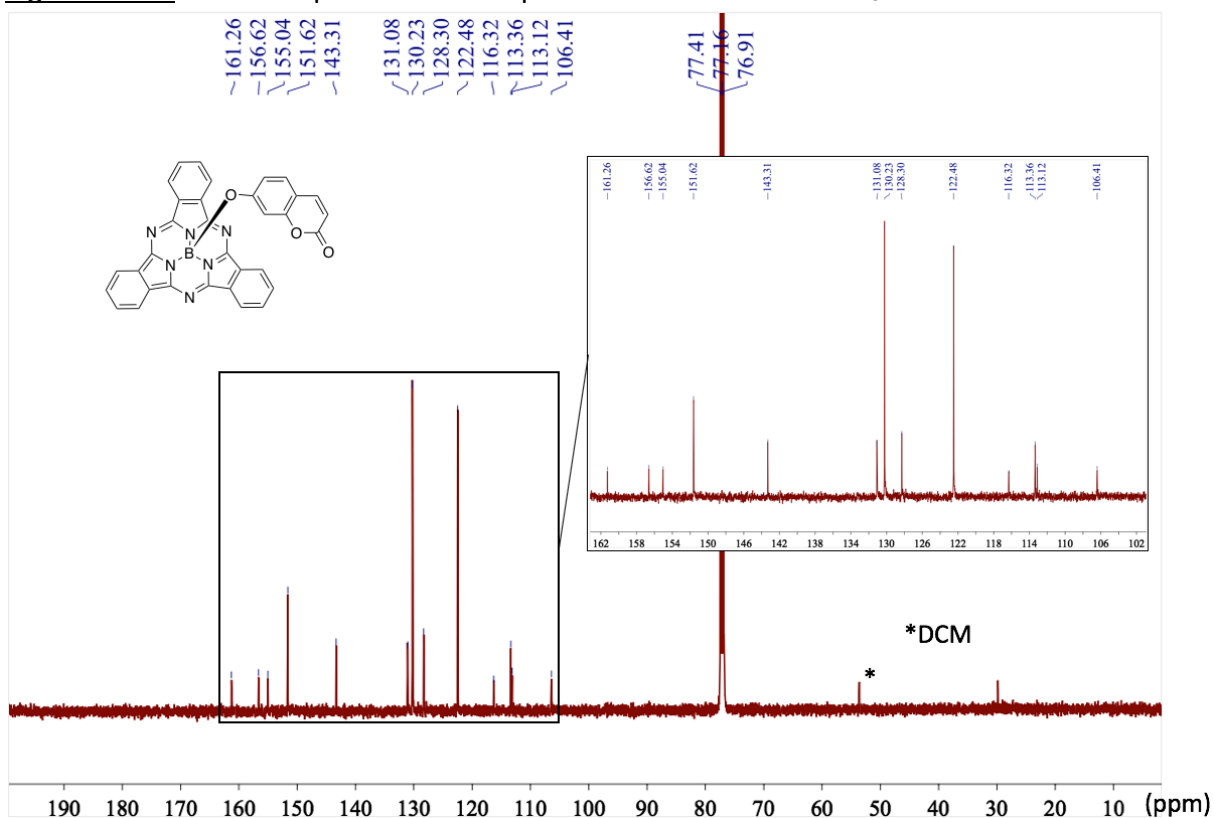


Figure S1-11: ^{13}C NMR spectrum of compound **06** recorded in CDCl_3 at 125 MHz and 300 K



II. RP-HPLC elution profiles of compounds 01, 03, 04, 05 and 06

HPLC-MS analyses were performed on a Thermo-Dionex Ultimate 3000 instrument equipped with a diode array detector (Thermo-Dionex, FLD 3400-RS).

HPLC system used: RP-HPLC-MS (Phenomenex Kinetex C₁₈ column, 2.6 μm , 2.1 \times 50 mm) with MeCN (+ 0.1% FA) and 0.1% aq. formic acid (aq. FA, pH 2.7) as eluents [5% MeCN (0.1 min) followed by linear gradient from 5% to 100% (5 min) of MeCN and maintained at 100% during 3 min] at a flow rate of 0.5 mL min⁻¹. UV-visible detection was achieved at 220, 260 and 560 nm (+ DAD in the range 220-700 nm). Low resolution ESI-MS detection in the positive/negative mode (full scan, 100-1000 a.m.u., data type: centroid, needle voltage: 3.0 kV, probe temperature: 350 °C, cone voltage: 75 V and scan time: 1 s).

Figure S2-1: RP-HPLC elution profile of compound **01** at 560 nm

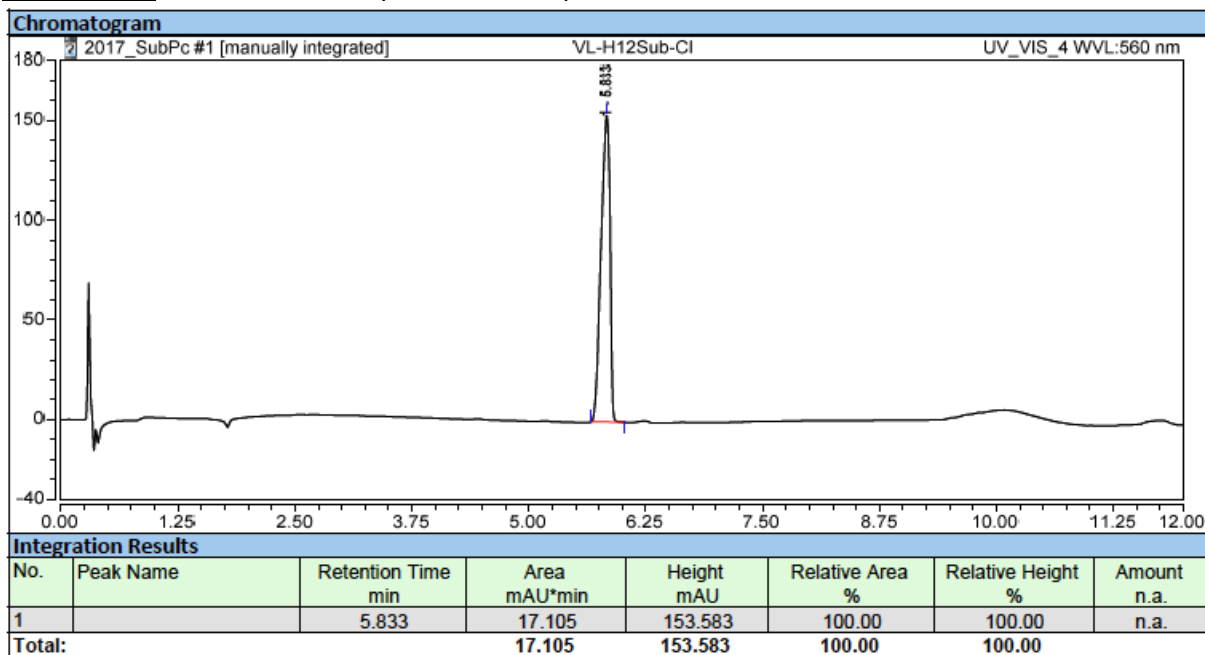


Figure S2-2: RP-HPLC elution profile of compound **03** at 560 nm

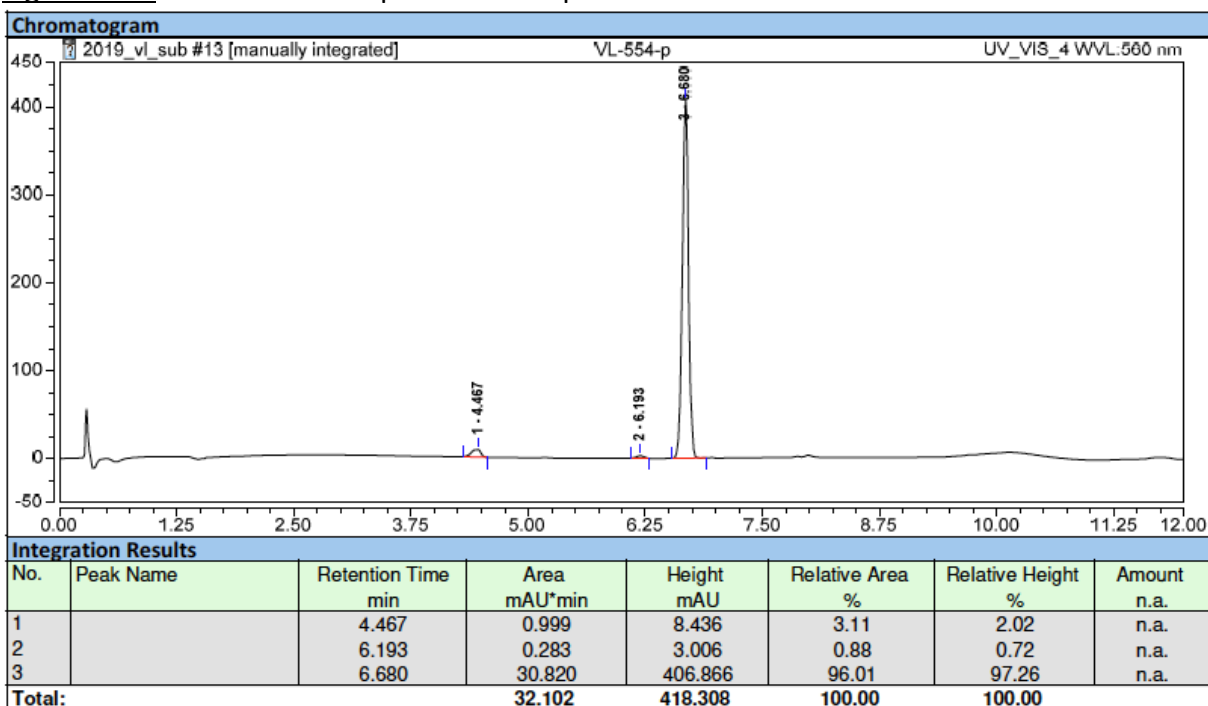


Figure S2-3: RP-HPLC elution profile of compound **04** at 560 nm

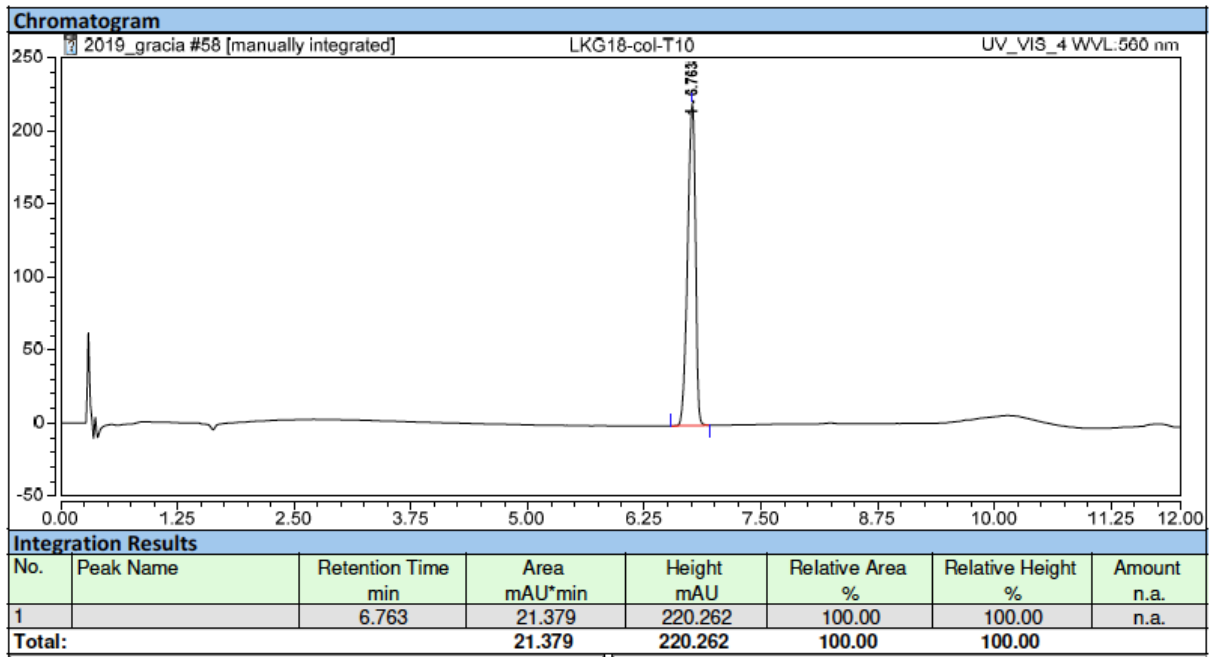


Figure S2-4: RP-HPLC elution profile of compound **05** at 560 nm

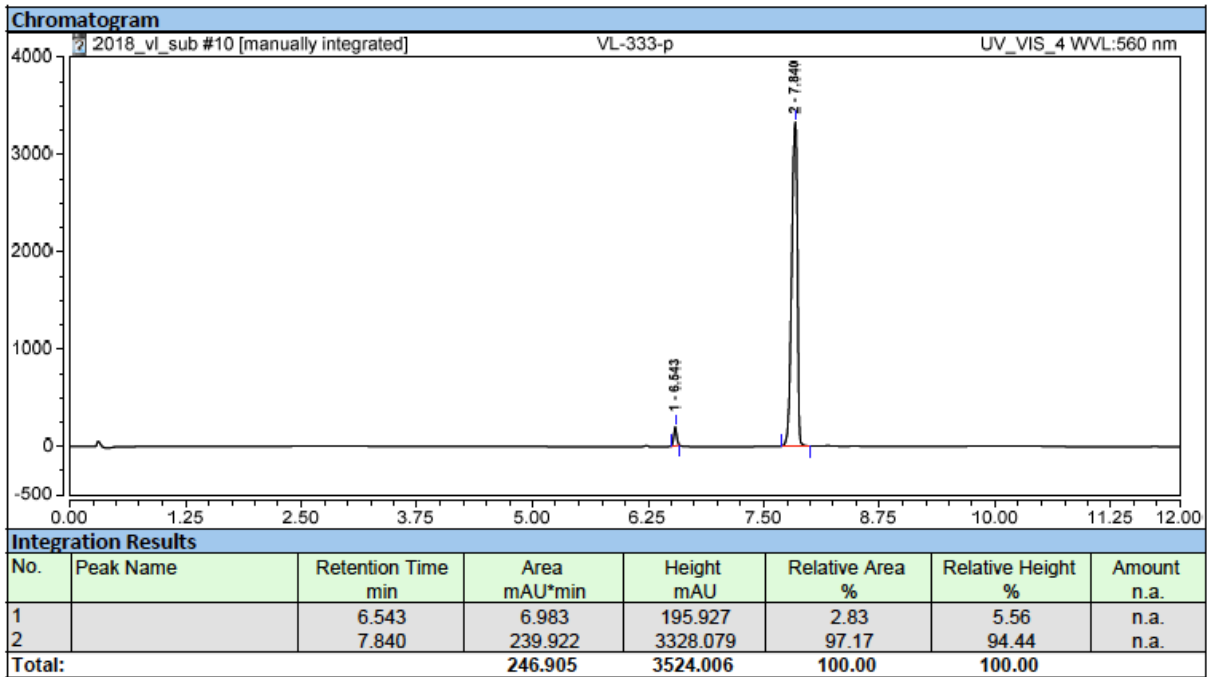
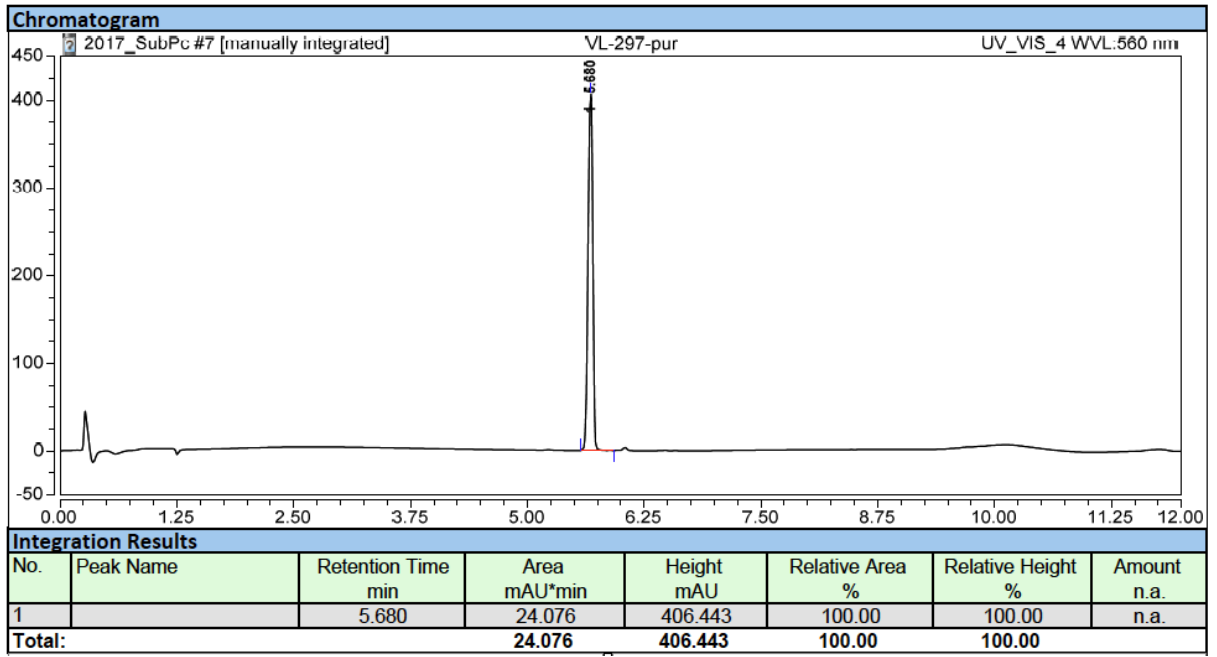


Figure S2-5: RP-HPLC elution profile of compound **06** at 560 nm



III. HRMS analysis

Figure S3-1: HRMS spectrum of compound **01**

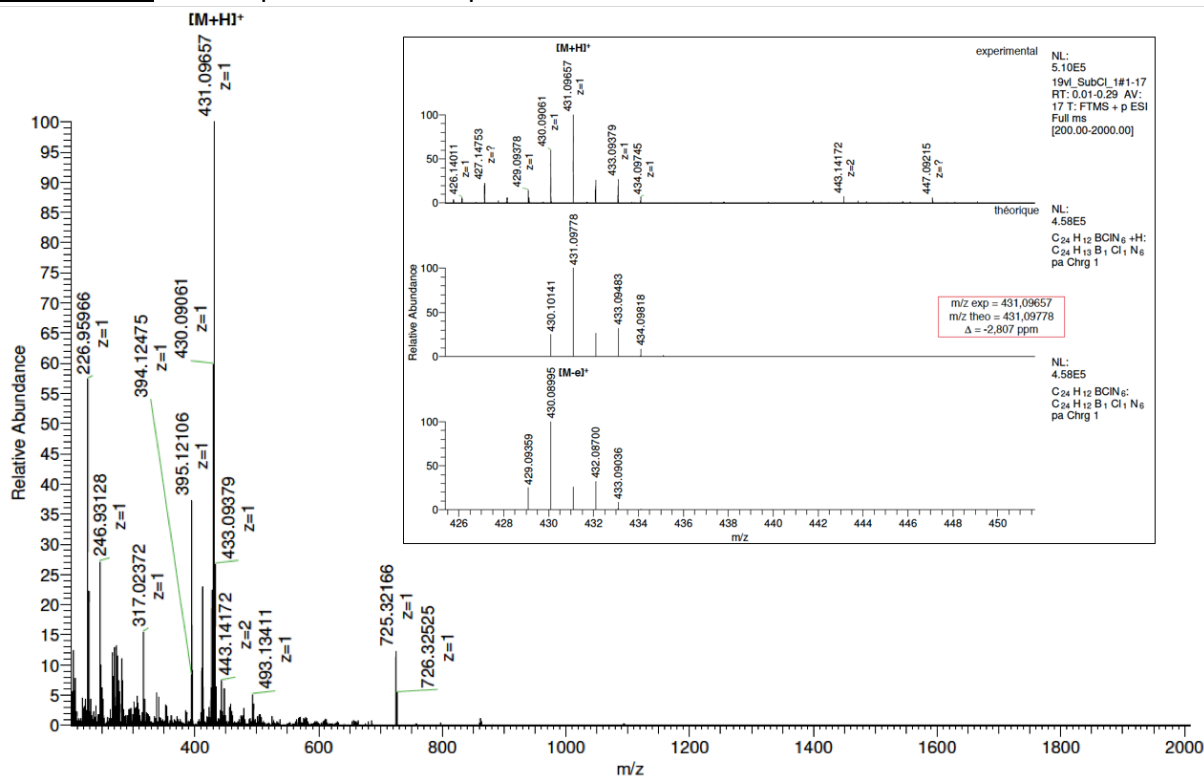


Figure S3-2: HRMS spectrum of compound **02**

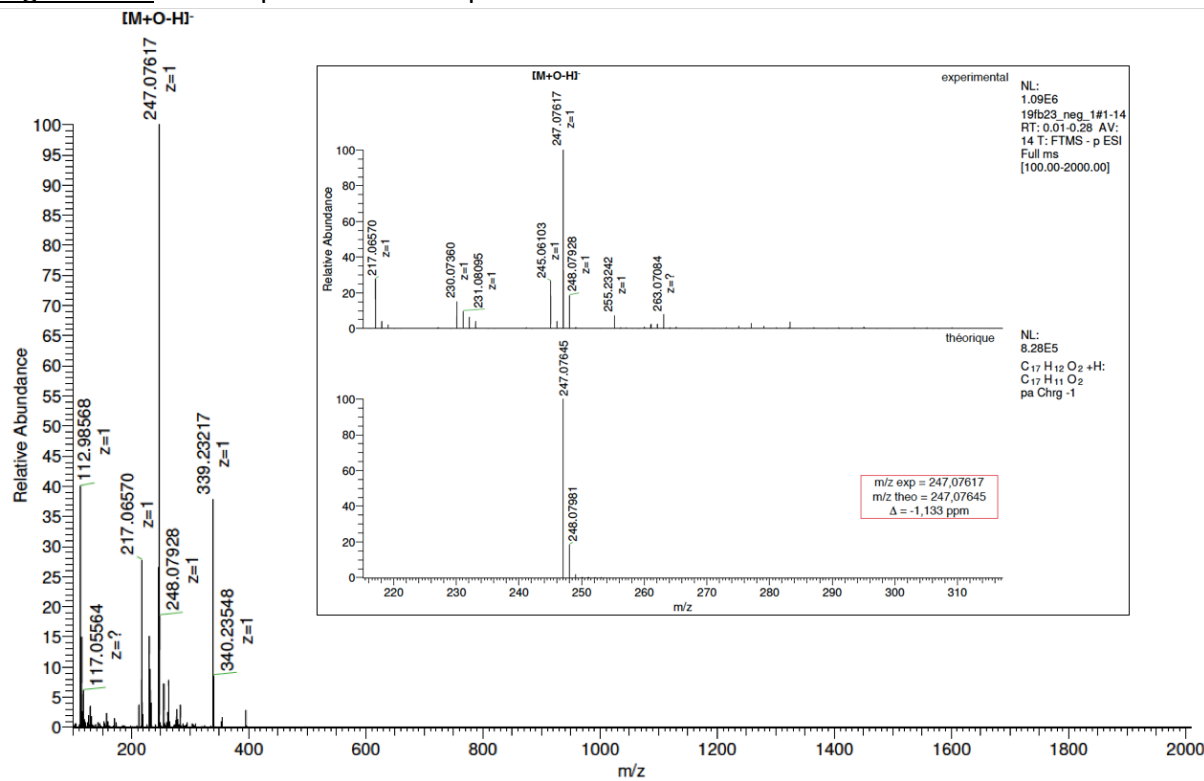


Figure S3-3: HRMS spectrum of compound **03**

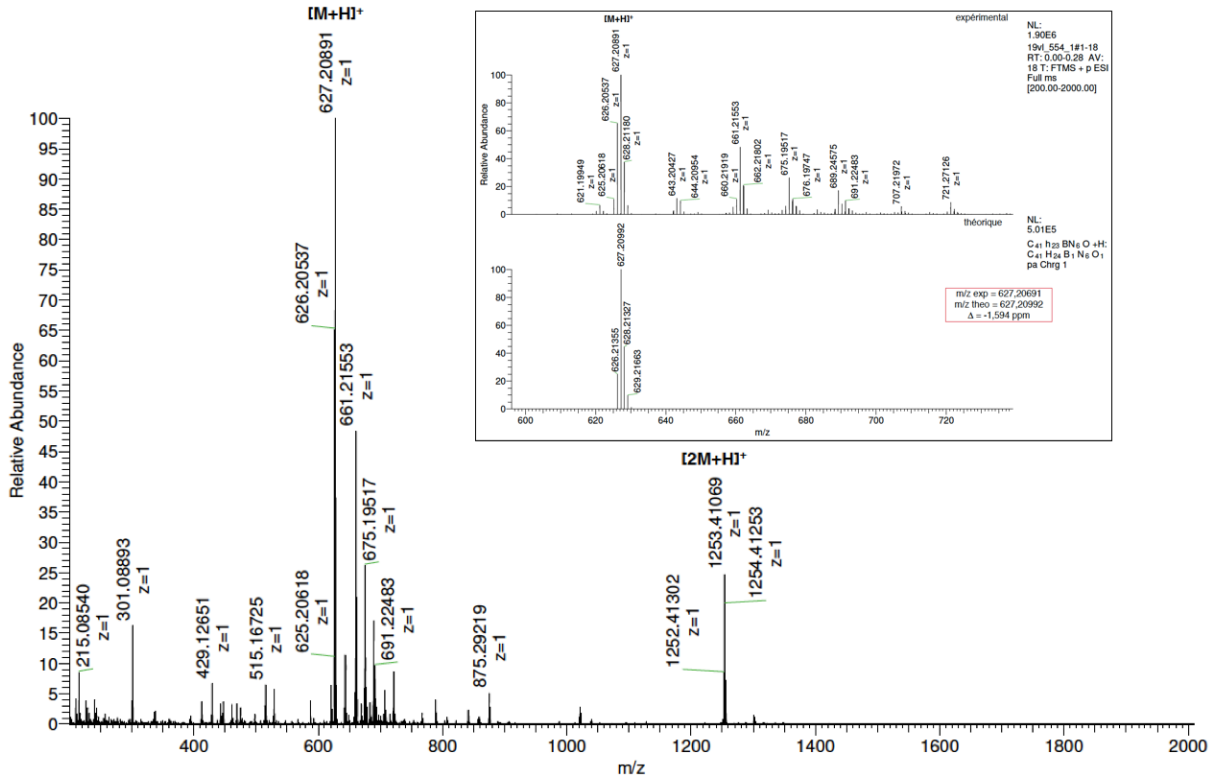


Figure S3-4: HRMS spectrum of compound **04**

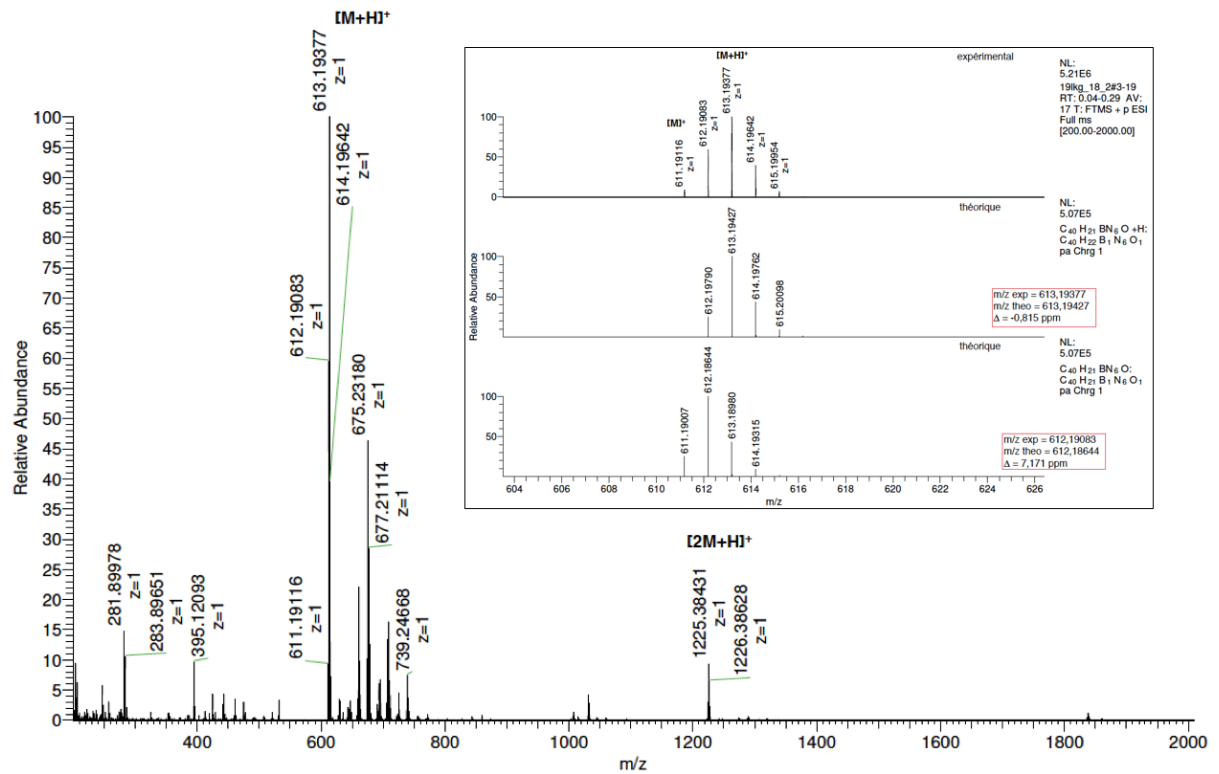


Figure S3-5: HRMS spectrum of compound **05**

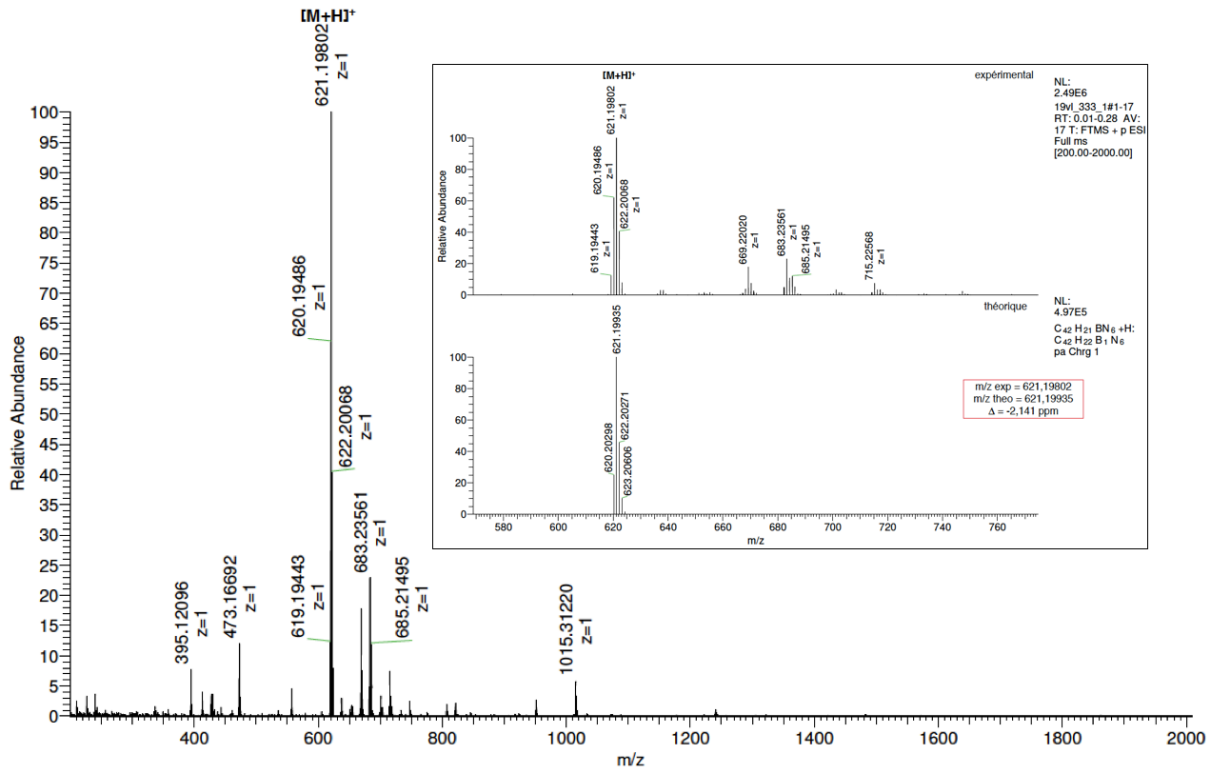
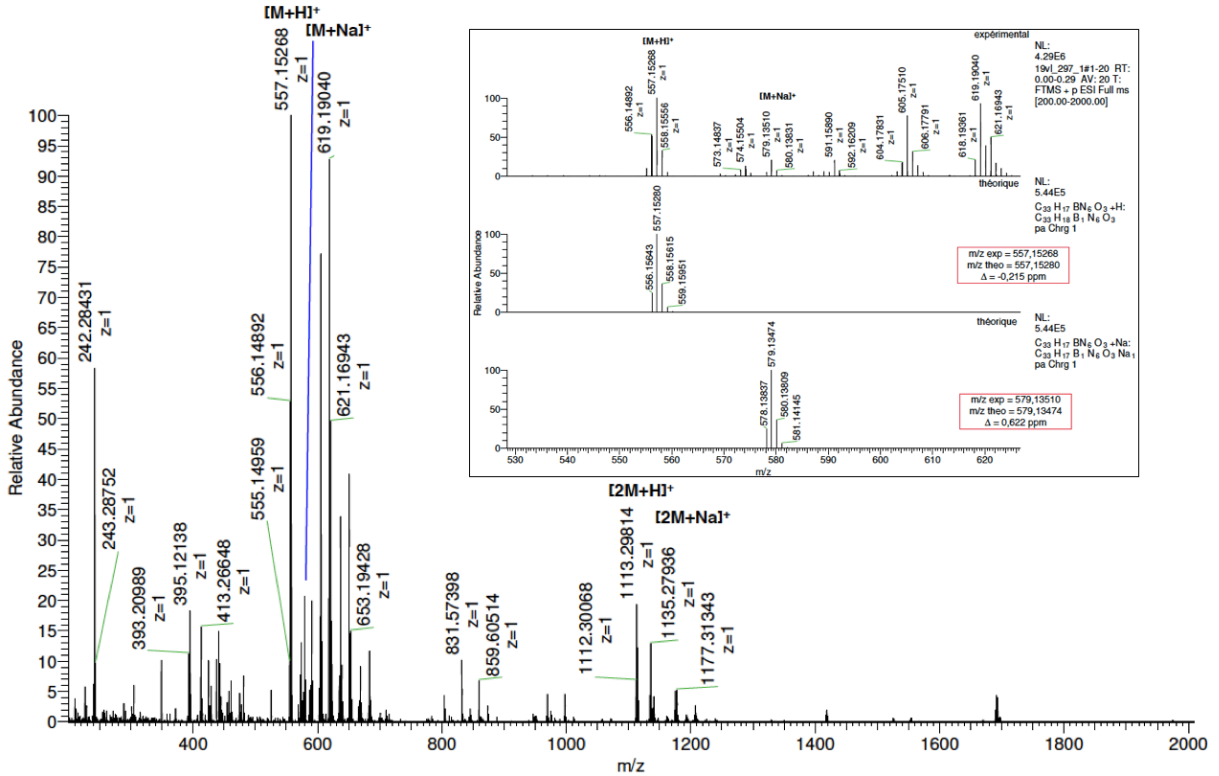


Figure S3-6: HRMS spectrum of compound **06**



IV. Absorbance, excitation and emission spectra of compounds 01, 03, 04, 05 and 06 in different solvents

Figure S4-1: Absorbance, excitation ($\lambda_{em} = 630$ nm) and emission ($\lambda_{ex} = 488$ nm) spectra of compound **01** in different solvents

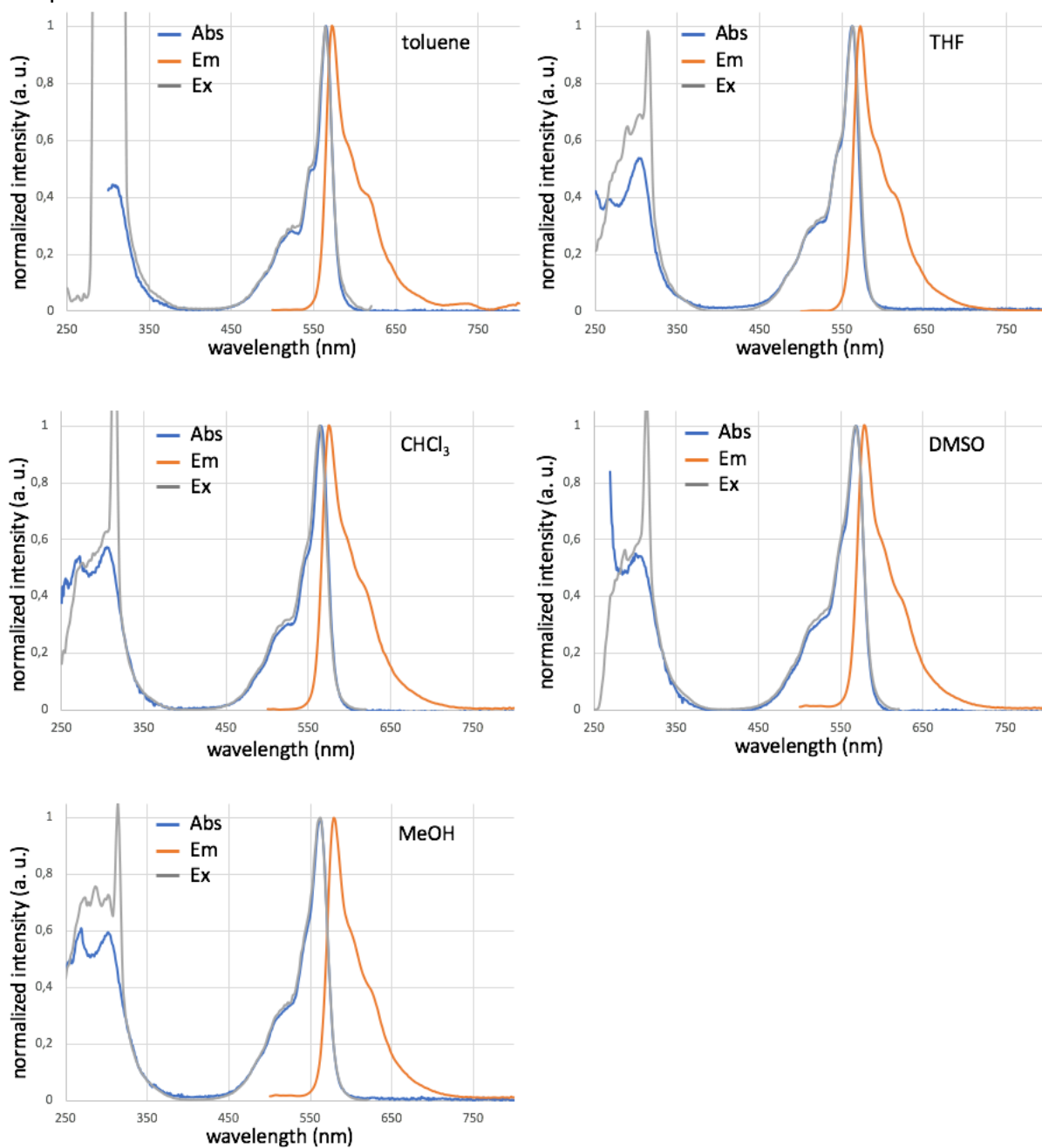


Figure S4-2: Absorbance, excitation ($\lambda_{em}= 630$ nm) and emission ($\lambda_{ex}= 488$ nm) spectra of compound **03** in different solvents

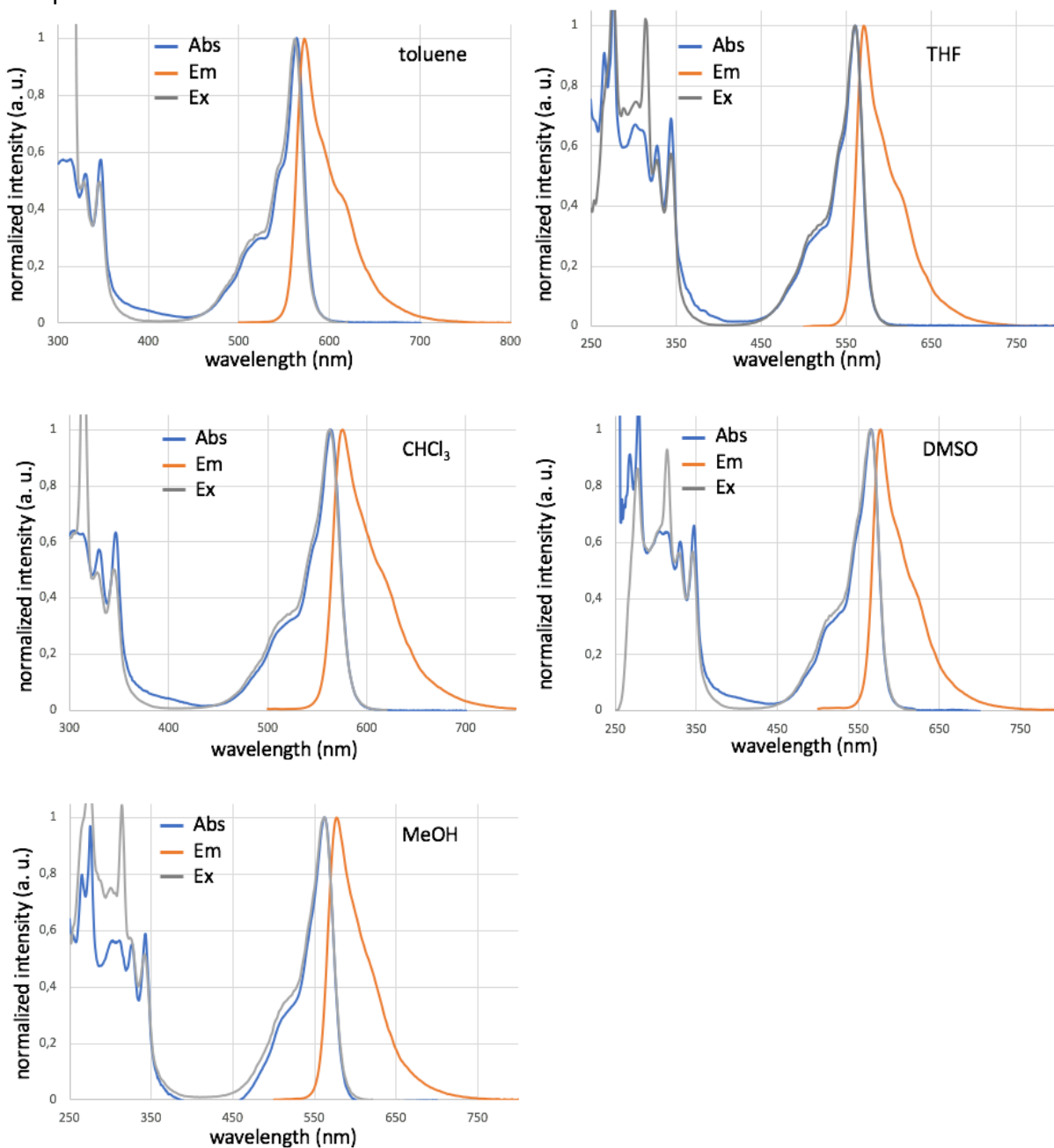


Figure S4-3: Absorbance, excitation ($\lambda_{em} = 630$ nm) and emission ($\lambda_{ex} = 488$ nm) spectra of compound **04** in different solvents

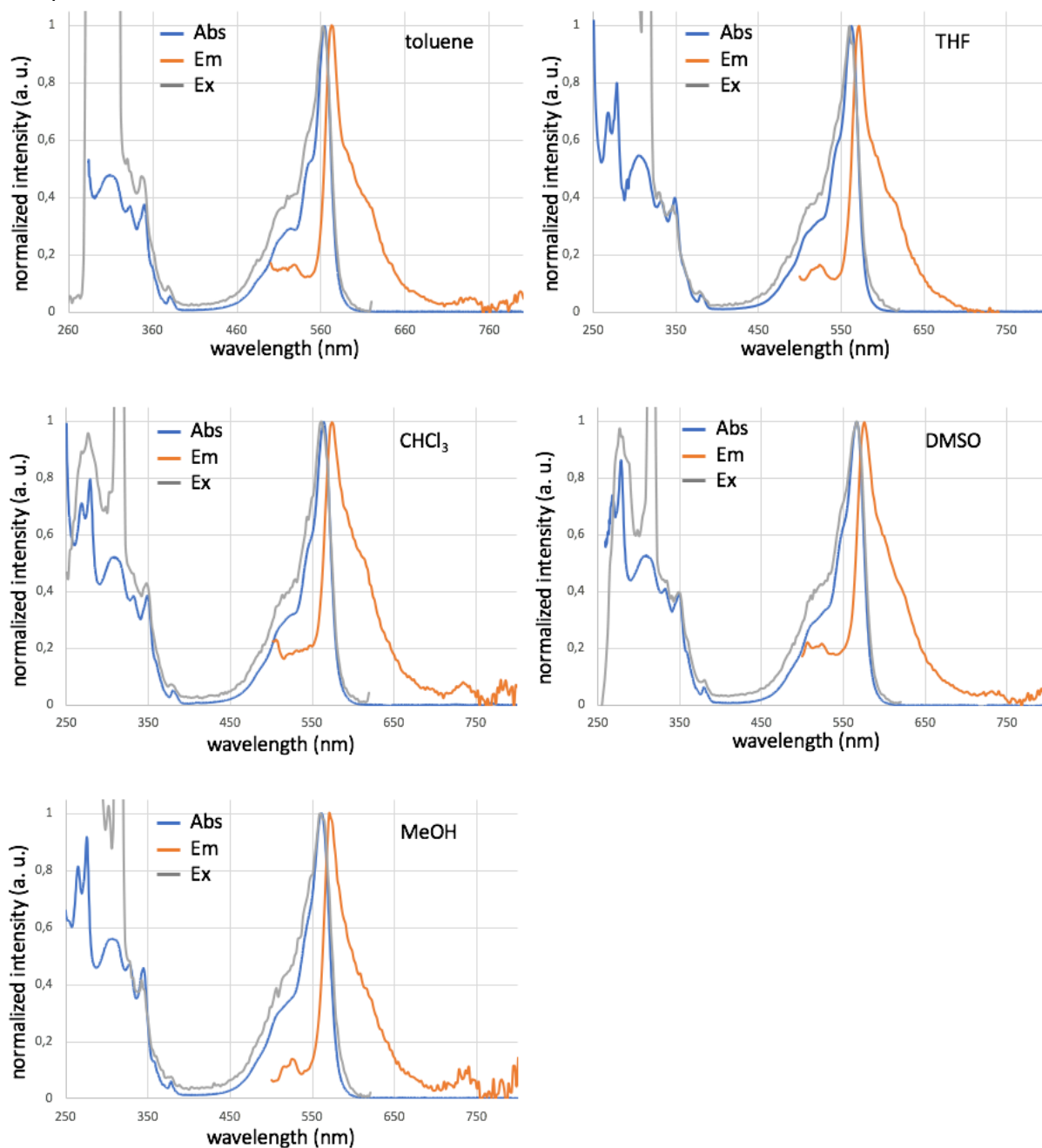


Figure S4-4: Absorbance, excitation ($\lambda_{em} = 630$ nm) and emission ($\lambda_{ex} = 488$ nm) spectra of compound **05** in different solvents

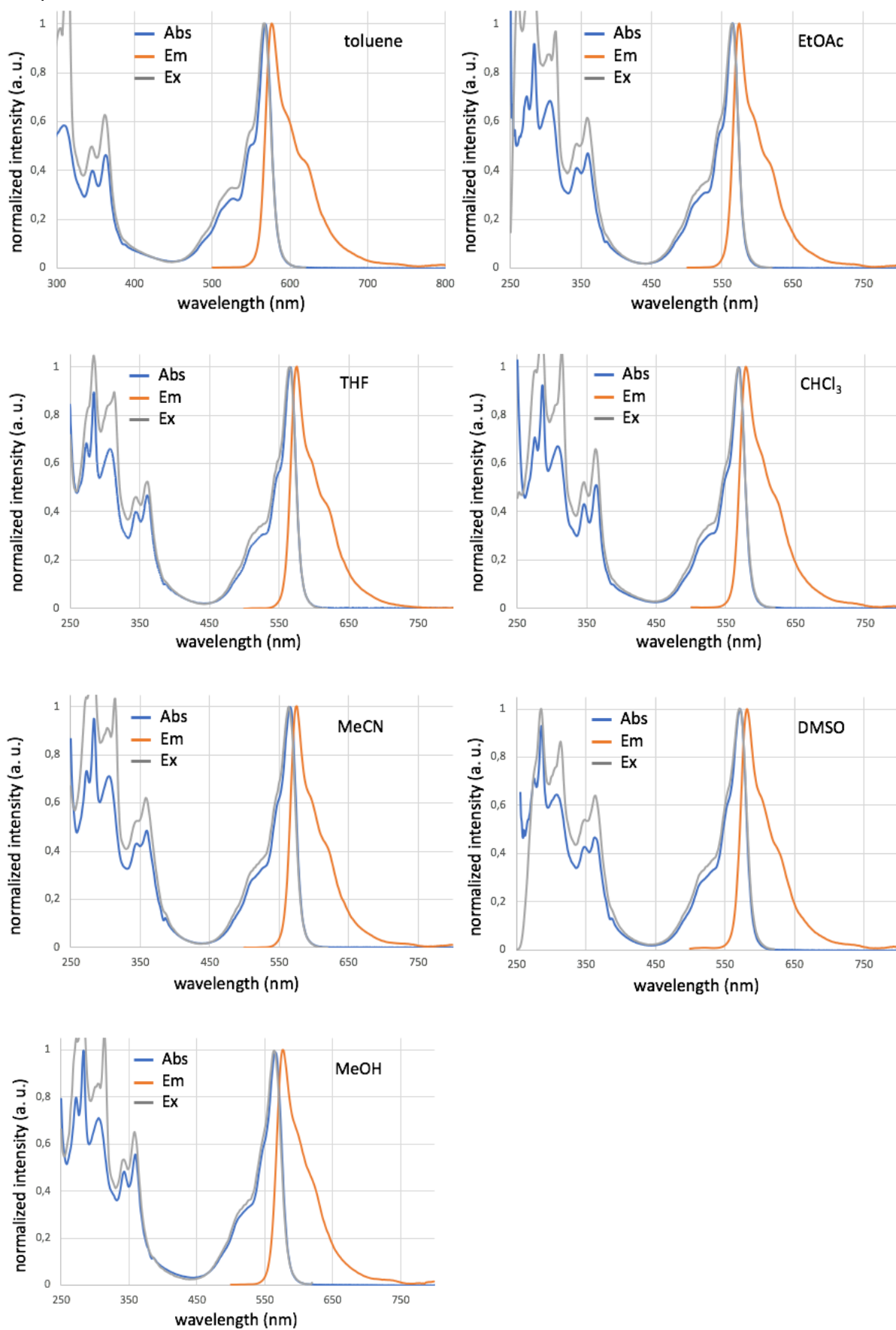
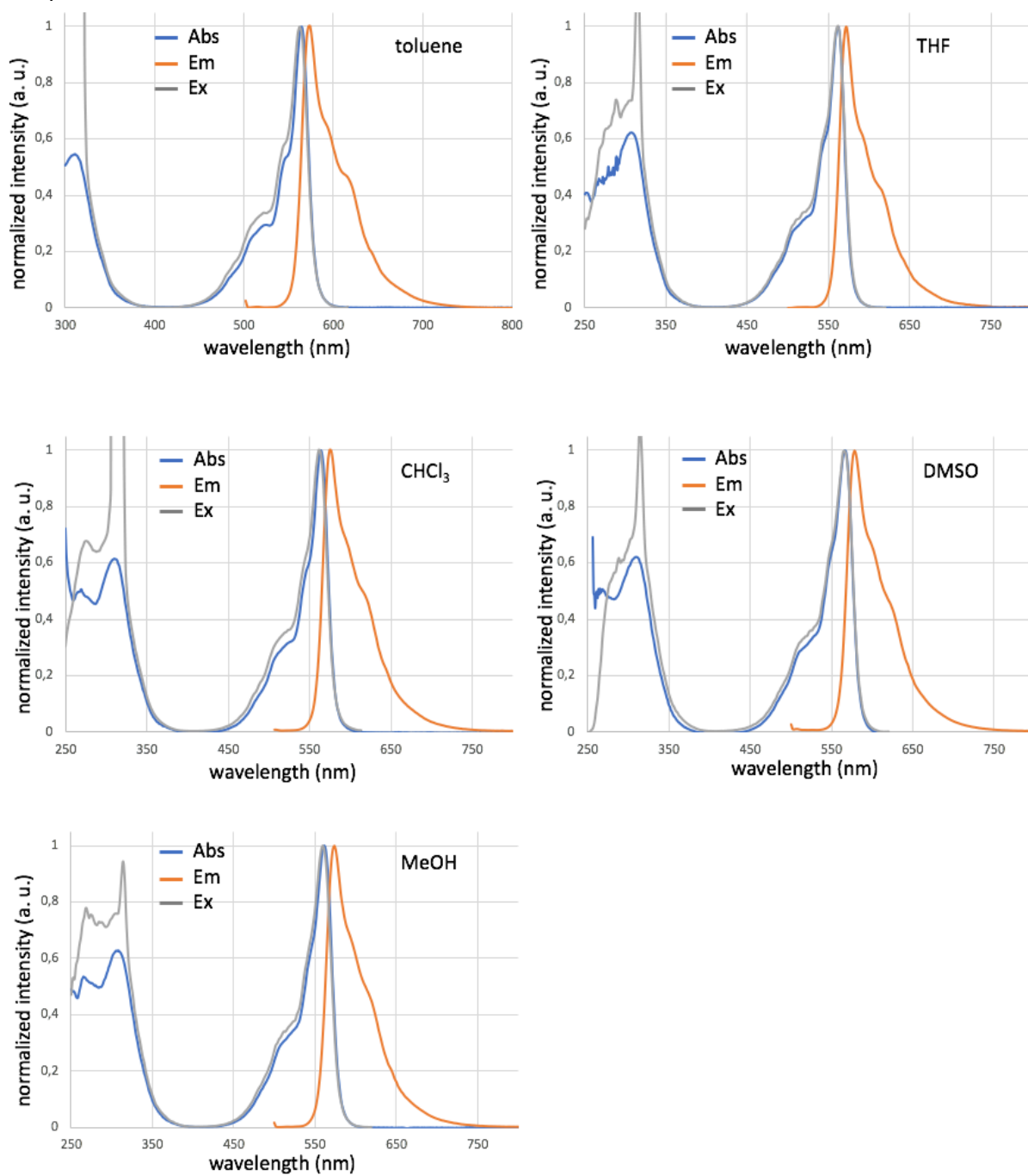


Figure S4-5: Absorbance, excitation ($\lambda_{em} = 630$ nm) and emission ($\lambda_{ex} = 488$ nm) spectra of compound **06** in different solvents



V. Energy Transfer Efficiency studies of compounds **03** and **05** in different solvents

Figure S5-1: Energy transfer efficiency of compound **03** in different solvents

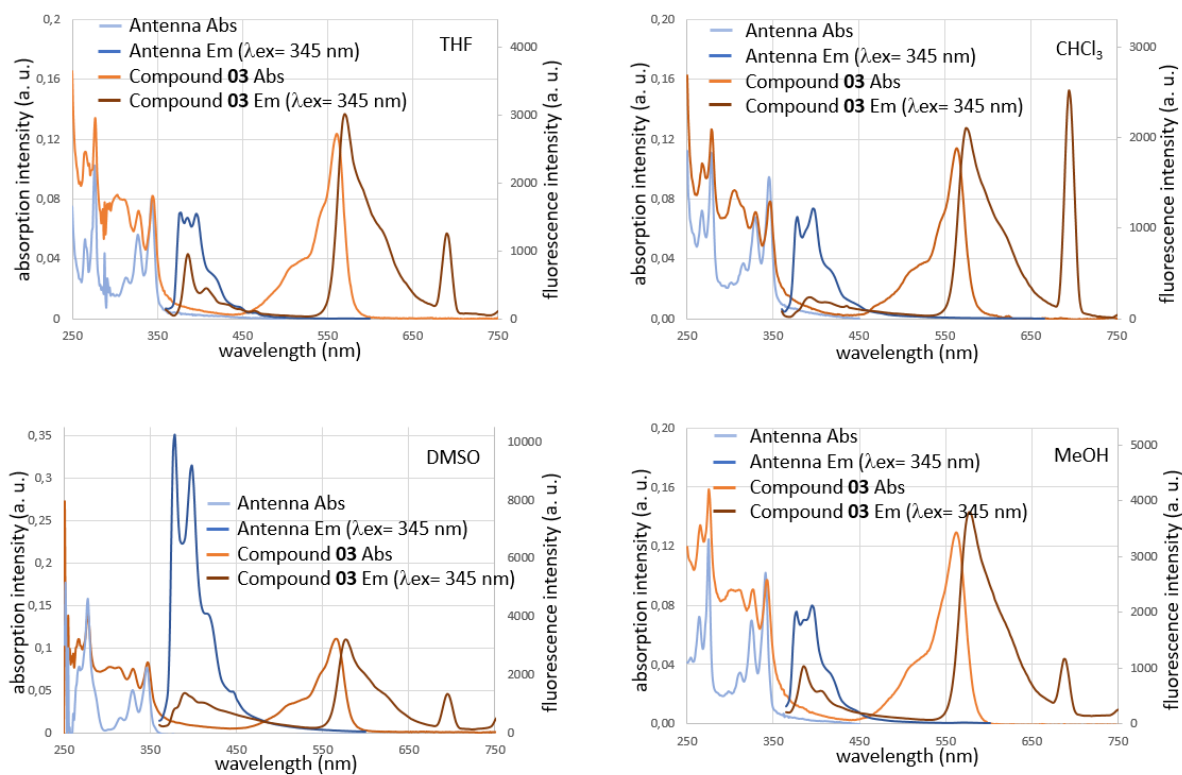
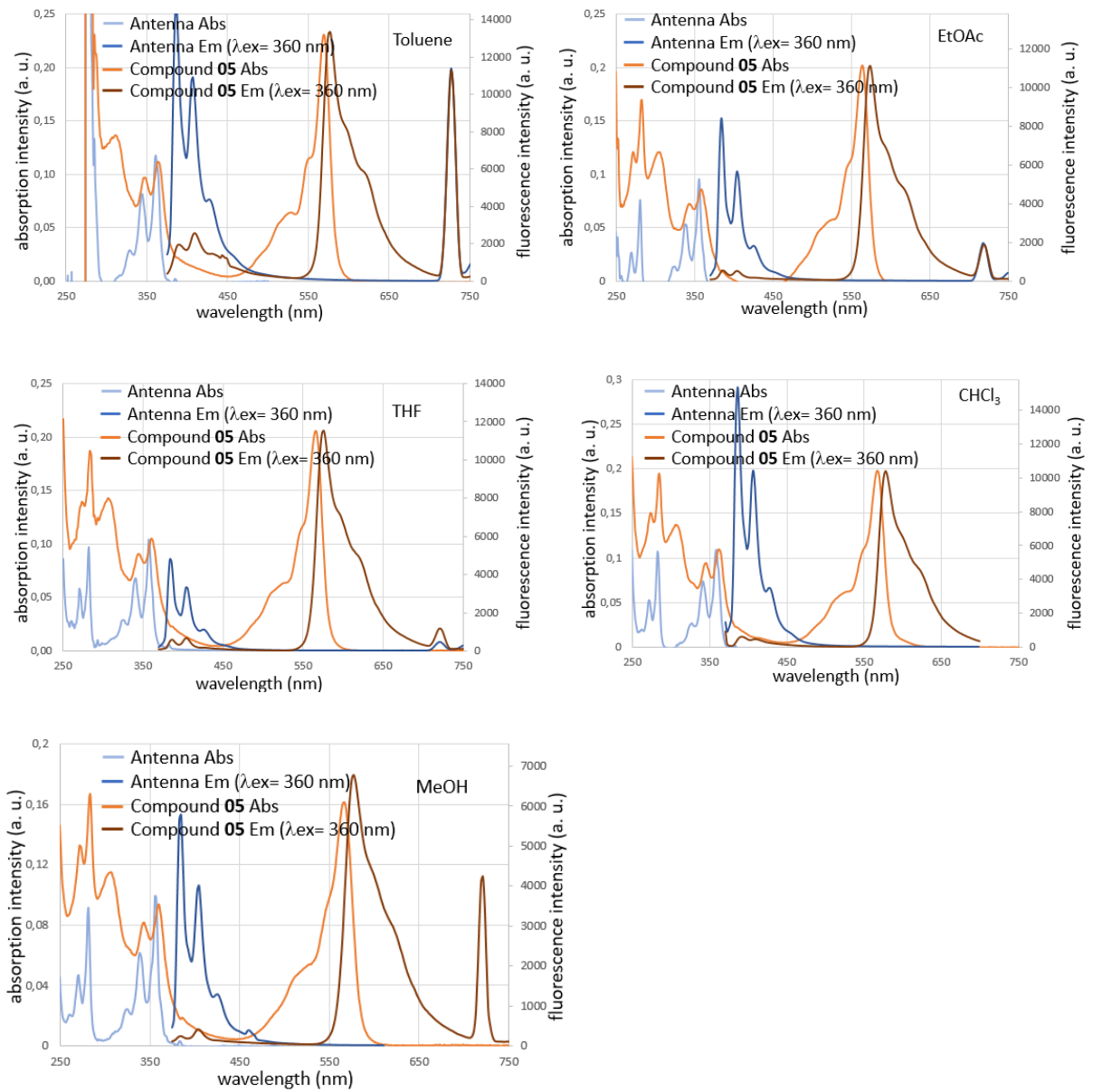


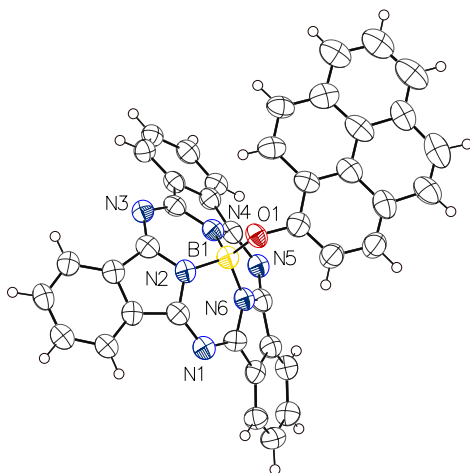
Figure S5-2: Energy transfer efficiency of compound **05** in different solvents



VI. X-Ray diffraction informations of compounds 4 and 6

Figure S6-1: X-Ray diffraction informations of compound 4

Crystal Data and Experimental



Experimental. Single clear light red plate-shaped crystals of compound **4** were recrystallized from a mixture of DCM and cyclohexane by slow evaporation. A suitable crystal 0.35x0.10x0.06 mm³ was selected and mounted on a MITIGEN holder oil on a Bruker D8 Venture diffractometer. The crystal was kept at a steady $T = 100.0(1)$ K during data collection. The structure was solved with the **ShelXT** (Sheldrick, 2015) structure solution program using the Intrinsic Phasing solution method and by using **Olex2** (Dolomanov et al., 2009) as the graphical interface. The model was refined with version 2018/3 of **ShelXL** (Sheldrick, 2015) using Least Squares minimization.

Crystal Data. C₄₀H₂₁BN₆O, $M_r = 612.44$, triclinic, $P-1$ (No. 2), $a = 9.9592(4)$ Å, $b = 12.1772(5)$ Å, $c = 13.5700(6)$ Å, $\alpha = 113.192(2)^\circ$, $\beta = 96.701(3)^\circ$, $\gamma = 103.825(2)^\circ$, $V = 1427.34(11)$ Å³, $T = 100.0(1)$ K, $Z = 2$, $Z' = 1$, $\mu(\text{CuK}\alpha) = 0.700$, 18696 reflections measured, 5023 unique ($R_{int} = 0.1053$) which were used in all calculations. The final wR_2 was 0.2813 (all data) and R_1 was 0.1041 ($I > 2(I)$).

Compound	4
CCDC	2005981
Internal Reference	20191125VLS4bOP
	y
Formula	C ₄₀ H ₂₁ BN ₆ O
$D_{calc.}/\text{g cm}^{-3}$	1.425
μ/mm^{-1}	0.700
Formula Weight	612.44
Color	clear light red
Shape	plate
Size/mm ³	0.35x0.10x0.06
T/K	100.0(1)
Crystal System	triclinic
Space Group	$P-1$
$a/\text{Å}$	9.9592(4)
$b/\text{Å}$	12.1772(5)
$c/\text{Å}$	13.5700(6)
$\alpha/^\circ$	113.192(2)
$\beta/^\circ$	96.701(3)
$\gamma/^\circ$	103.825(2)
$V/\text{Å}^3$	1427.34(11)
Z	2
Z'	1
Wavelength/Å	1.541840
Radiation type	CuK α
$\theta_{min}/^\circ$	3.647
$\theta_{max}/^\circ$	66.941
Measured Refl.	18696
Independent Refl.	5023
Reflections with $I > 2(I)$	3266
R_{int}	0.1053
Parameters	433
Restraints	0
Largest Peak	0.468
Deepest Hole	-0.359
GooF	1.048
wR_2 (all data)	0.2813
wR_2	0.2523
R_1 (all data)	0.1462
R_1	0.1041

Structure Quality Indicators

Reflections:	d min (Cu) 0.84	I/σ 11.4	R _{int} 10.53%	complete 99%
Refinement:	Shift 0.000	Max Peak 0.5	Min Peak -0.4	Goof 1.048

A clear light red plate-shaped crystal with dimensions 0.35x0.10x0.06 mm³ was mounted on a MITIGEN holder oil. Data were collected using a Bruker D8 Venture diffractometer equipped with an Oxford Cryosystems low-temperature device operating at $T = 100.0(1)$ K. Data were measured using ϕ and ω scans' using CuK α radiation. The total number of runs and images was based on the strategy calculation from the program APEX3 (Bruker, 2015) The maximum resolution that was achieved was $\theta = 66.941^\circ$ (0.84 Å). The diffraction pattern was indexed. The total number of runs and images was based on the strategy calculation from the program APEX3 (Bruker, 2015) and the unit cell was refined using **SAINT** (Bruker, V8.40A, after 2013) on 4970 reflections, 27% of the observed reflections. Data reduction, scaling and absorption corrections were performed using **SAINT** (Bruker, V8.40A, after 2013). The final completeness is 98.70 % out to 66.941° in θ . A multi-scan absorption correction was performed using **SADABS-2016/2** (Bruker,2016) was used for absorption correction. $wR_2(\text{int})$ was 0.1218 before and 0.0935 after correction. The Ratio of minimum to maximum transmission is 0.8010. The absorption coefficient μ of this material is 0.700 mm⁻¹ at this wavelength ($\lambda = 1.542\text{Å}$) and the minimum and maximum transmissions are 0.733 and 0.915. The structure was solved and the space group $P-1$ (# 2) determined by the **ShelXT** (Sheldrick, 2015) structure solution program using Intrinsic Phasing and refined by Least Squares using version 2018/3 of **ShelXL** (Sheldrick, 2015). All non-hydrogen atoms were refined anisotropically. Hydrogen atom positions were calculated geometrically and refined using the riding model. Hydrogen atom positions were calculated geometrically and refined using the riding model. There is a single molecule in the asymmetric unit, which is represented by the reported sum formula. In other words: Z is 2 and Z' is 1.

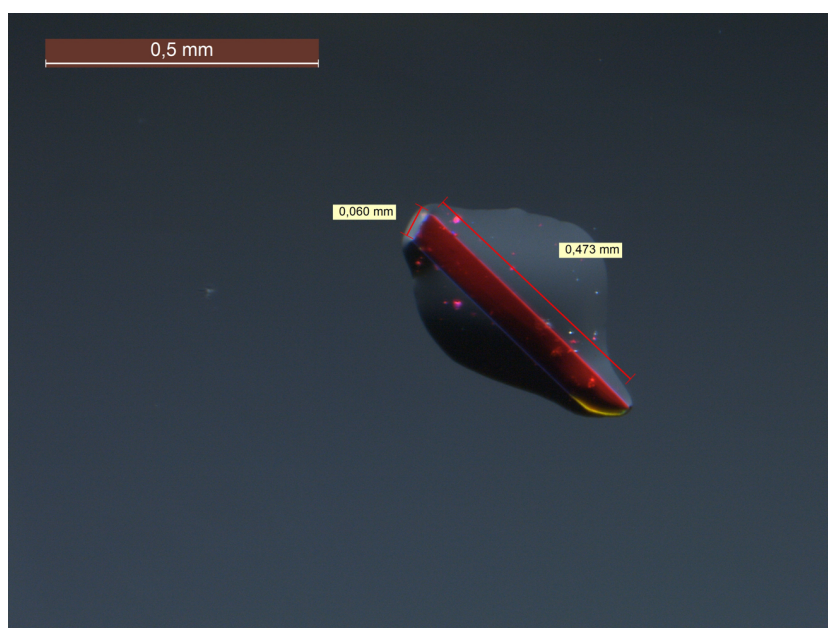


Figure 1: View of selected sample.

Table 1: Bond Lengths in Å for compound **4**.

Atom	Atom	Length/Å	Atom	Atom	Length/Å
O1	C9	1.374(7)	C4A	C5A	1.404(7)
O1	B1	1.430(7)	C4B	C5B	1.386(8)
N1	C1	1.355(6)	C5	C6	1.392(7)
N1	C8B	1.342(7)	C5A	C6A	1.389(7)
N2	C1B	1.358(7)	C5B	C6B	1.380(8)
N2	C8B	1.372(7)	C6	C7	1.386(7)
N2	B1	1.496(7)	C6A	C7A	1.405(7)
N3	C1B	1.353(7)	C6B	C7B	1.387(7)
N3	C8A	1.346(6)	C7	C8	1.458(7)
N4	C1A	1.357(6)	C7A	C8A	1.452(7)
N4	C8A	1.365(6)	C7B	C8B	1.472(7)
N4	B1	1.499(7)	C9	C10	1.379(8)
N5	C1A	1.339(7)	C9	C14	1.397(8)
N5	C8	1.351(7)	C10	C11	1.392(9)
N6	C1	1.372(6)	C11	C12	1.349(9)
N6	C8	1.368(6)	C12	C13	1.470(9)
N6	B1	1.499(7)	C12	C15	1.422(9)
C1	C2	1.456(7)	C13	C14	1.402(8)
C1A	C2A	1.459(7)	C13	C24	1.392(8)
C1B	C2B	1.443(7)	C14	C23	1.474(8)
C2	C3	1.395(7)	C15	C16	1.312(9)
C2	C7	1.433(7)	C16	C17	1.483(10)
C2A	C3A	1.386(7)	C17	C18	1.354(9)
C2A	C7A	1.426(7)	C17	C24	1.434(8)
C2B	C3B	1.398(7)	C18	C19	1.373(11)
C2B	C7B	1.426(7)	C19	C20	1.385(10)
C3	C4	1.381(8)	C20	C21	1.401(9)
C3A	C4A	1.388(7)	C21	C22	1.442(9)
C3B	C4B	1.385(8)	C21	C24	1.446(9)
C4	C5	1.396(8)	C22	C23	1.347(8)

Table 2: Bond Angles in ° for compound **04**.

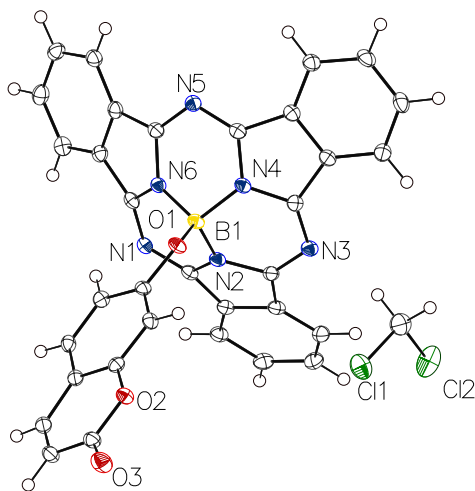
Atom	Atom	Atom	Angle/°	Atom	Atom	Atom	Angle/°
C9	O1	B1	117.0(4)	C7	C2	C1	106.7(5)
C8B	N1	C1	117.0(4)	C3A	C2A	C1A	132.5(5)
C1B	N2	C8B	112.6(4)	C3A	C2A	C7A	121.0(5)
C1B	N2	B1	122.6(4)	C7A	C2A	C1A	106.4(4)
C8B	N2	B1	123.3(4)	C3B	C2B	C1B	132.6(5)
C8A	N3	C1B	115.9(4)	C3B	C2B	C7B	119.9(5)
C1A	N4	C8A	113.4(4)	C7B	C2B	C1B	107.3(5)
C1A	N4	B1	123.7(4)	C4	C3	C2	117.6(5)
C8A	N4	B1	122.2(4)	C2A	C3A	C4A	118.0(5)
C1A	N5	C8	115.9(4)	C4B	C3B	C2B	117.9(5)
C1	N6	B1	123.3(4)	C3	C4	C5	122.5(5)
C8	N6	C1	112.3(4)	C3A	C4A	C5A	121.6(5)
C8	N6	B1	123.0(4)	C3B	C4B	C5B	121.5(5)
N1	C1	N6	122.1(5)	C6	C5	C4	120.6(5)
N1	C1	C2	129.3(5)	C6A	C5A	C4A	121.1(5)
N6	C1	C2	106.5(4)	C6B	C5B	C4B	122.0(5)
N4	C1A	C2A	105.8(4)	C7	C6	C5	118.2(5)
N5	C1A	N4	122.9(5)	C5A	C6A	C7A	117.9(5)
N5	C1A	C2A	129.8(5)	C5B	C6B	C7B	117.6(5)
N2	C1B	C2B	107.0(4)	C2	C7	C8	106.9(4)
N3	C1B	N2	123.4(5)	C6	C7	C2	120.8(5)
N3	C1B	C2B	128.0(5)	C6	C7	C8	132.0(5)
C3	C2	C1	132.4(5)	C2A	C7A	C8A	107.5(5)
C3	C2	C7	120.2(5)	C6A	C7A	C2A	120.3(5)

Atom	Atom	Atom	Angle/°
C6A	C7A	C8A	131.9(5)
C2B	C7B	C8B	106.4(5)
C6B	C7B	C2B	121.1(5)
C6B	C7B	C8B	132.0(5)
N5	C8	N6	123.3(5)
N5	C8	C7	128.2(5)
N6	C8	C7	106.5(4)
N3	C8A	N4	123.1(5)
N3	C8A	C7A	130.7(5)
N4	C8A	C7A	105.2(4)
N1	C8B	N2	122.6(5)
N1	C8B	C7B	129.7(5)
N2	C8B	C7B	105.5(4)
O1	C9	C10	119.7(6)
O1	C9	C14	120.1(5)
C10	C9	C14	120.2(6)
C9	C10	C11	120.5(6)
C12	C11	C10	121.7(6)
C11	C12	C13	119.0(6)
C11	C12	C15	125.1(7)
C15	C12	C13	115.8(6)
C14	C13	C12	118.2(5)
C24	C13	C12	119.5(6)
C24	C13	C14	122.3(6)
C9	C14	C13	120.2(5)

Atom	Atom	Atom	Angle/°
C9	C14	C23	120.9(5)
C13	C14	C23	118.8(5)
C16	C15	C12	125.0(7)
C15	C16	C17	121.6(6)
C18	C17	C16	123.4(7)
C18	C17	C24	121.8(7)
C24	C17	C16	114.7(6)
C17	C18	C19	119.3(8)
C18	C19	C20	121.8(7)
C19	C20	C21	121.6(8)
C20	C21	C22	123.0(6)
C20	C21	C24	116.8(7)
C22	C21	C24	120.1(6)
C23	C22	C21	120.8(6)
C22	C23	C14	119.9(6)
C13	C24	C17	123.4(7)
C13	C24	C21	118.0(6)
C17	C24	C21	118.6(6)
O1	B1	N2	110.9(4)
O1	B1	N4	116.1(5)
O1	B1	N6	117.6(5)
N2	B1	N4	104.2(4)
N2	B1	N6	103.7(4)
N4	B1	N6	102.8(4)

Figure S6-2: X-Ray diffraction informations of compound **6**

Crystal Data and Experimental



Experimental. Single clear light red prism-shaped crystals of compound **6** were recrystallized from DCM by slow evaporation. A suitable crystal 0.50x0.24x0.10 mm³ was selected and mounted on a MITIGEN holder oil on a Bruker D8 Venture diffractometer. The crystal was kept at a steady $T = 100.0(1)$ K during data collection. The structure was solved with the **ShelXT** (Sheldrick, 2015) structure solution program using the Intrinsic Phasing solution method and by using **Olex2** (Dolomanov et al., 2009) as the graphical interface. The model was refined with version 2018/3 of **ShelXL** (Sheldrick, 2015) using Least Squares minimization.

Crystal Data. C₃₄H₁₉BCl₂N₆O₃, $M_r = 641.26$, monoclinic, $P2_1/c$ (No. 14), $a = 11.2700(6)$ Å, $b = 16.3338(9)$ Å, $c = 15.6723(6)$ Å, $\beta = 101.100(3)^\circ$, $\alpha = \gamma = 90^\circ$, $V = 2831.0(2)$ Å³, $T = 100.0(1)$ K, $Z = 4$, $Z' = 1$, $\mu(\text{CuK}\alpha) = 2.478$, 69277 reflections measured, 5018 unique ($R_{int} = 0.0599$) which were used in all calculations. The final wR_2 was 0.0895 (all data) and R_1 was 0.0354 ($I > 2s(I)$).

Compound	6
CCDC	2005982
Internal Reference	20190502VL297
Formula	C ₃₄ H ₁₉ BCl ₂ N ₆ O ₃
$D_{calc.}/\text{g cm}^{-3}$	1.505
μ/mm^{-1}	2.478
Formula Weight	641.26
Colour	clear light red
Shape	prism
Size/mm ³	0.50x0.24x0.10
T/K	100.0(1)
Crystal System	monoclinic
Space Group	$P2_1/c$
$a/\text{Å}$	11.2700(6)
$b/\text{Å}$	16.3338(9)
$c/\text{Å}$	15.6723(6)
$\alpha/^\circ$	90
$\beta/^\circ$	101.100(3)
$\gamma/^\circ$	90
$V/\text{Å}^3$	2831.0(2)
Z	4
Z'	1
Wavelength/Å	1.541840
Radiation type	CuK α
$\theta_{min}/^\circ$	3.948
$\theta_{max}/^\circ$	66.797
Measured Refl.	69277
Independent Refl.	5018
Reflections with $I > 2(I)$	4461
R_{int}	0.0599
Parameters	415
Restraints	0
Largest Peak	0.241
Deepest Hole	-0.391
GooF	1.069
wR_2 (all data)	0.0895
wR_2	0.0861
R_1 (all data)	0.0409
R_1	0.0354

Structure Quality Indicators

Reflections:	d min (Cu)	0.84	I/σ	43.5	Rint	5.99%	complete	100%
Refinement:	Shift	0.001	Max Peak	0.2	Min Peak	-0.4	Goof	1.069

A clear light red prism-shaped crystal with dimensions 0.50x0.24x0.10 mm³ was mounted on a MITIGEN holder oil. Data were collected using a Bruker D8 Venture diffractometer equipped with an Oxford Cryosystems low-temperature device operating at $T = 100.0(1)$ K. Data were measured using ϕ and ω scans using CuK α radiation. The total number of runs and images was based on the strategy calculation from the program APEX3 (Bruker, 2015) The maximum resolution that was achieved was $\Theta = 66.797^\circ$ (0.84 Å). The diffraction pattern was indexed. The total number of runs and images was based on the strategy calculation from the program APEX3 (Bruker, 2015) and the unit cell was refined using **SAINT** (Bruker, V8.38A, after 2013) on 2267 reflections, 3% of the observed reflections. Data reduction, scaling and absorption corrections were performed using **SAINT** (Bruker, V8.38A, after 2013). The final completeness is 99.80 % out to 66.797° in Θ . A multi-scan absorption correction was performed using **SADABS-2016/2** (Bruker, 2016) was used for absorption correction. $wR_2(\text{int})$ was 0.1162 before and 0.0766 after correction. The Ratio of minimum to maximum transmission is 0.7194. The absorption coefficient μ of this material is 2.478 mm⁻¹ at this wavelength ($\lambda = 1.542\text{Å}$) and the minimum and maximum transmissions are 0.447 and 0.621. The structure was solved and the space group $P2_1/c$ (# 14) determined by the **ShelXT** (Sheldrick, 2015) structure solution program using Intrinsic Phasing and refined by Least Squares using version 2018/3 of **ShelXL** (Sheldrick, 2015). All non-hydrogen atoms were refined anisotropically. Hydrogen atom positions were calculated geometrically and refined using the riding model. Hydrogen atom positions were calculated geometrically and refined using the riding model. There is a single molecule in the asymmetric unit, which is represented by the reported sum formula. In other words: Z is 4 and Z' is 1.

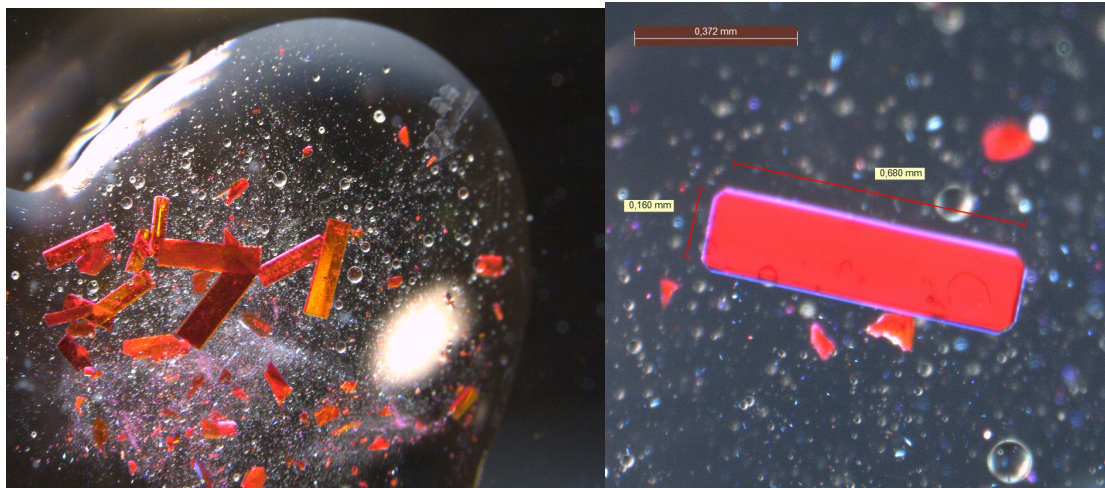


Figure 2: View of sample batch (left) and selected crystal (right).

Table 3: Bond Lengths in Å for compound **6**.

Atom	Atom	Length/Å	Atom	Atom	Length/Å
Cl1	C34	1.775(2)	N1	C10	1.350(2)
Cl2	C34	1.767(2)	N1	C33	1.343(2)
O1	C1	1.355(2)	N2	C10	1.370(2)
O1	B1	1.449(2)	N2	C17	1.367(2)
O2	C7	1.387(2)	N2	B1	1.496(2)
O2	C8	1.381(2)	N3	C17	1.349(2)
O3	C7	1.206(2)	N3	C18	1.343(2)

Atom	Atom	Length/Å	Atom	Atom	Length/Å
N4	C18	1.362(2)	C13	C14	1.403(3)
N4	C25	1.364(2)	C14	C15	1.383(3)
N4	B1	1.489(2)	C15	C16	1.394(3)
N5	C25	1.348(2)	C16	C17	1.455(2)
N5	C26	1.342(2)	C18	C19	1.460(2)
N6	C26	1.369(2)	C19	C20	1.390(2)
N6	C33	1.369(2)	C19	C24	1.426(2)
N6	B1	1.495(2)	C20	C21	1.384(3)
C1	C2	1.401(2)	C21	C22	1.400(3)
C1	C9	1.391(2)	C22	C23	1.386(3)
C2	C3	1.380(2)	C23	C24	1.391(2)
C3	C4	1.402(3)	C24	C25	1.459(2)
C4	C5	1.432(2)	C26	C27	1.458(2)
C4	C8	1.396(2)	C27	C28	1.393(3)
C5	C6	1.344(3)	C27	C32	1.419(2)
C6	C7	1.451(3)	C28	C29	1.389(3)
C8	C9	1.380(2)	C29	C30	1.395(3)
C10	C11	1.453(2)	C30	C31	1.390(3)
C11	C12	1.397(2)	C31	C32	1.392(2)
C11	C16	1.425(2)	C32	C33	1.457(2)
C12	C13	1.387(3)			

Table 4: Bond Angles in ° for compound 6.

Atom	Atom	Atom	Angle/°	Atom	Atom	Atom	Angle/°
C12	C34	C11	110.90(11)	C16	C11	C10	107.07(15)
C1	O1	B1	126.22(13)	C13	C12	C11	117.92(16)
C8	O2	C7	122.09(14)	C12	C13	C14	121.41(16)
C33	N1	C10	117.38(14)	C15	C14	C13	121.21(17)
C10	N2	B1	123.29(14)	C14	C15	C16	118.39(17)
C17	N2	C10	112.74(14)	C11	C16	C17	107.09(15)
C17	N2	B1	122.08(14)	C15	C16	C11	120.38(16)
C18	N3	C17	117.10(15)	C15	C16	C17	132.29(16)
C18	N4	C25	113.89(14)	N2	C17	C16	105.91(14)
C18	N4	B1	122.44(14)	N3	C17	N2	122.77(15)
C25	N4	B1	123.35(15)	N3	C17	C16	129.53(16)
C26	N5	C25	116.68(14)	N3	C18	N4	122.23(15)
C26	N6	C33	112.83(14)	N3	C18	C19	130.74(16)
C26	N6	B1	122.44(14)	N4	C18	C19	105.52(14)
C33	N6	B1	123.30(14)	C20	C19	C18	132.51(16)
O1	C1	C2	123.66(16)	C20	C19	C24	120.66(16)
O1	C1	C9	116.14(15)	C24	C19	C18	106.79(15)
C9	C1	C2	120.18(16)	C21	C20	C19	117.91(17)
C3	C2	C1	119.82(16)	C20	C21	C22	121.56(17)
C2	C3	C4	121.10(16)	C23	C22	C21	121.21(17)
C3	C4	C5	124.39(16)	C22	C23	C24	117.99(17)
C8	C4	C3	117.57(16)	C19	C24	C25	107.45(15)
C8	C4	C5	118.04(16)	C23	C24	C19	120.61(16)
C6	C5	C4	120.82(17)	C23	C24	C25	131.89(16)
C5	C6	C7	121.29(16)	N4	C25	C24	105.21(14)
O2	C7	C6	116.83(15)	N5	C25	N4	122.00(15)
O3	C7	O2	116.21(16)	N5	C25	C24	131.43(16)
O3	C7	C6	126.96(17)	N5	C26	N6	123.12(16)
O2	C8	C4	120.74(15)	N5	C26	C27	129.91(16)
C9	C8	O2	116.80(15)	N6	C26	C27	105.51(14)
C9	C8	C4	122.46(16)	C28	C27	C26	131.91(16)
C8	C9	C1	118.84(15)	C28	C27	C32	120.59(16)
N1	C10	N2	122.36(15)	C32	C27	C26	107.40(15)
N1	C10	C11	129.76(15)	C29	C28	C27	117.94(17)
N2	C10	C11	105.91(14)	C28	C29	C30	121.27(17)
C12	C11	C10	132.11(16)	C31	C30	C29	121.60(17)
C12	C11	C16	120.65(16)	C30	C31	C32	117.57(17)

Atom	Atom	Atom	Angle/°
C27	C32	C33	107.01(15)
C31	C32	C27	120.96(16)
C31	C32	C33	131.95(16)
N1	C33	N6	122.45(16)
N1	C33	C32	130.20(16)
N6	C33	C32	105.74(14)

Atom	Atom	Atom	Angle/°
O1	B1	N2	116.52(15)
O1	B1	N4	107.80(14)
O1	B1	N6	118.25(15)
N4	B1	N2	104.57(14)
N4	B1	N6	103.66(14)
N6	B1	N2	104.52(14)

Citations

O.V. Dolomanov and L.J. Bourhis and R.J. Gildea and J.A.K. Howard and H. Puschmann, Olex2: A complete structure solution, refinement and analysis program, *J. Appl. Cryst.*, (2009), **42**, 339-341.

Sheldrick, G.M., Crystal structure refinement with ShelXL, *Acta Cryst.*, (2015), **C71**, 3-8.

Sheldrick, G.M., ShelXT-Integrated space-group and crystal-structure determination, *Acta Cryst.*, (2015), **A71**, 3-8.

Software for the Integration of CCD Detector System Bruker Analytical X-ray Systems, Bruker AXS, Madison, WI (after 2013).